The Astrophysical Journal, 942:57 (16pp), 2023 January 10 https://doi.org/10.3847/1538-4357/aca3a5

Photosynthetic Fluorescence from Earthlike Planets around Sunlike and Cool Stars

Yu Komatsu[1,2], Yasunori Hori[1,2], Masayuki Kuzuhara[1,2], Makiko Kosugi[1,2,3], Kenji Takizawa[1,3], Norio Narita[1,4,5], Masashi Omiya[1,2], Eunchul Kim[3], Nobuhiko Kusakabe[1,2], Victoria Meadows[6,7], and Motohide Tamura[1,2,8]
[1] Astrobiology Center, 2-21-1 Osawa, Mitaka, Tokyo 181-8588, Japan; yu.komatsu@nao.ac.jp
[2] National Astronomical Observatory of Japan, 2-21-1 Osawa, Mitaka, Tokyo 181-8588, Japan
[3] National Institute for Basic Biology, 38 Nishigonaka, Myodaiji, Okazaki, Aichi 444-8585, Japan
[4] Komaba Institute for Science, The University of Tokyo, 3-8-1 Komaba, Meguro, Tokyo 153-8902, Japan
[5] Instituto de Astrofísica de Canarias (IAC), E-38205 La Laguna, Tenerife, Spain
[6] Department of Astronomy and Astrobiology Program, University of Washington, Box 351580, Seattle, WA 98195, USA
[7] NASA Nexus for Exoplanet System Science, Virtual Planetary Laboratory Team, Box 351580, University of Washington, Seattle, WA 98195, USA
[8] Department of Astronomy, Graduate School of Science, The University of Tokyo, 7-3-1, Hongo, Bunkyo-ku, Tokyo 113-0033, Japan
Received 2022 August 15; revised 2022 November 12; accepted 2022 November 15; published 2023 January 11

Abstract

Remote sensing of the Earth has demonstrated that photosynthesis is traceable as the vegetation red edge (VRE), which is a steep rise in the reflection spectrum of vegetation, and as solar-induced fluorescence. This study examines the detectability of biological fluorescence from two types of photosynthetic pigments, chlorophylls (Chls) and bacteriochlorophylls (BChls), on Earthlike planets with oxygen-rich/poor and anoxic atmospheres around the Sun and M dwarfs. Atmospheric absorption, such as H_2O, CH_4, O_2, and O_3, and the VRE obscure the fluorescence emissions from Chls and BChls. We find that the BChl-based fluorescence for wavelengths of 1000–1100 nm, assuming the spectrum of BChl *b*–bearing purple bacteria, could provide a suitable biosignature, but only in the absence of water cloud coverage or other strong absorbers near 1000 nm. The Chl fluorescence is weaker for several reasons, e.g., spectral blending with the VRE. The apparent reflectance excess is greatly increased in both the Chl and BChl cases around TRAPPIST-1, due to the fluorescence and stellar absorption lines. This could be a promising feature for detecting the fluorescence around ultracool red dwarfs using follow-up ground-based observations at high spectral resolution; however, this would require a long time around Sunlike stars, even for a LUVOIR-like space mission. Moreover, the simultaneous detection of fluorescence and the VRE is the key to identifying traces of photosynthesis, because absorption, reflectance, and fluorescence are physically connected. For further validation of the fluorescence detection, the nonlinear response of biological fluorescence as a function of light intensity could be considered.

Unified Astronomy Thesaurus concepts: Astrobiology (74); Exoplanet surfaces (2118); Biosignatures (2018)

1. Introduction

The ultimate goal of characterizing rocky planets is to identify potential biosignatures, spectral fingerprints of atmospheric gases, and surface features produced by biological activities (Des Marais et al. 2002; Meadows et al. 2018; Schwieterman et al. 2018). The simultaneous identification of oxygen, ozone, and methane on rocky habitable planets shows promise as a way of detecting Earthlike life. Oxygenic photosynthesis produces a unique feature in the reflection spectrum on a planetary surface, called the vegetation red edge (VRE), as well as biosignature gases (Kiang et al. 2007a). The VRE is the steep difference in the reflection spectrum of the surface vegetation around 700 nm, due to chlorophyll (Chl) absorption in the visible region and the large reflectance by cell structures in the near-infrared (NIR) region (Gates & Schleter 1965; Jacquemoud & Baret 1990). Remote sensing of the Earth and earthshine observations provides the spectral indices that are involved in the VRE, such as the NDVI, which is the normalized difference in the reflection spectrum of the Earth between the visible and NIR wavelength regions. The Moderate Resolution Imaging Spectroradiometer on board NASA's Terra satellite has shown that, at 16 day intervals at 500 m and 1 km resolutions, the NDVI varies from 0.05 to nearly 0.9, with the upper limit being obtained at a dense forest site during the peak growing season (Huete et al. 2002). Whereas remote sensing observes local areas on Earth, earthshine observations provide disk-averaged spectra of the Earth, leading to fruitful insights into exoplanet applications. The apparent reflectance change in the Earth's disk-averaged spectrum due to surface vegetation is less than 2% (Montañés-Rodríguez et al. 2006). The NDVI calculated from the earthshine observations varies by up to ∼0.10, depending on the different views of the Earth, and is reduced by cloud coverage (Tinetti et al. 2006). The application of the NDVI to disk-averaged spectra assuming Earthlike exoplanets requires caution, because remote sensing only observes local areas on the Earth for mapping vegetation. For instance, Livengood et al. (2011) found that spectral bands in addition to NDVI are required to distinguish between the Earth's vegetation and the Moon's surface.

The VRE signals from exoplanets around stars other than Sunlike stars are challenging to predict, due to the complexity of photosynthetic mechanisms in different light environments. However, the VRE on exoplanets may still be recognizable as anomalous and time-varying, due to the seasonal variability of the vegetation, and have a step-function-like spectroscopic feature at wavelengths different from those on the Earth (Seager et al. 2005). Tinetti et al. (2006) have proposed that if a three-photon photosynthetic scheme were working on

exoplanets around M dwarfs, and there were little or no visible light, then the red edge of the vegetation could be shifted into the NIR. However, according to Takizawa et al. (2017), even around M dwarfs, the evolution of photosynthesis in water may drive a preference for using visible light rather than the NIR, even after organisms colonize land surfaces. Moreover, the light absorption properties of land vegetation could be optimized after long-term adaptive evolution, depending on the stellar irradiations, as estimated by Lehmer et al. (2021). Anoxygenic photosynthesis, as performed by organisms such as purple bacteria, is thought to precede the emergence of oxygenic photosynthesis, whose global effect has been characterized by the great oxidation event (∼2.3 billion years ago (Ga)). Sanromá et al. (2013) have discussed the detectability of light reflected from purple bacteria with bacteriochlorophyll (BChl) as a photosynthetic pigment. They have shown that purple bacteria exhibit detectable features, and that their VRE peak is redder than that of higher plants, assuming an Earthlike planet before the rise of oxygen. In a comprehensive study of different pigment reflectivities, Schwieterman et al. (2015) showed that both nonphotosynthetic pigments and photosynthetic pigments affect the disk-averaged spectra. Furthermore, when it comes to false-positive detections, the reflectance features of some minerals on the Earth are similar to the VRE ones (Seager et al. 2005; Schwieterman 2018). Thus, extracting the VRE signal from reflected light should require knowledge of the surface environment on an exoplanet and high-resolution spectroscopic observations.

Fluorescence is another photosynthesis-related phenomenon that could also be a remote-sensing biosignature. Fluorescence is one of the de-excitation processes of photosynthetic pigments from the excited states to the ground state, along with intersystem crossing and inner conversion. Photosynthetic organisms on the Earth use Chls or BChls as light-absorbing pigments and electron donors/acceptors in the primary reactions of photosynthesis. The photon energy captured by Chls/BChls is mainly transferred to the reaction center (RC), which is the pigment-protein complex at the center of the photosystem used for photochemical reactions. However, some of the photon energy is dissipated as heat or emitted as fluorescence from light-harvesting antenna systems, which are pigment-protein complexes surrounding the RC that capture light energy and deliver the energy to the RC. Excess photon energy is preferentially removed as heat dissipation, rather than fluorescence. As a result, the fluorescence yield tends to be a smaller percentage of the excess energy and fluctuates with the degree of the excitation energy transfer between the Chls and heat dissipation. The fluorescence yield of photosynthetic organisms is estimated to be ∼5%, whereas that of free Chls/BChls in organic solvents is ∼30% (Grimm et al. 2006).

Plants and other oxygenic phototrophs use two different photosystems in sequence: photosystem II (PSII) and photosystem I (PSI). The energy level of the RC of PSII is higher, being equivalent to 680 nm, than that of PSI. In general, Chl fluorescence is mainly emitted from PSII, because the excess light energy in PSI is immediately dissipated as heat. Therefore, the fluorescence spectrum of a cell has a peak at 680 nm, and the distribution of the fluorescence emission extends to wavelengths up to 780 nm. Note that fluorescence emissions at 680 nm under highly concentrated Chl conditions, such as a leaf structure, decrease due to reabsorption by peripheral Chls with a red absorption band. Conversely, the six BChls (BChls *a*, *b*, *c*, *d*, *e*, and *g*) used in nonoxygenic photosynthetic bacteria, such as purple bacteria, green sulfur and nonsulfur bacteria, and heliobacteria (Kiang et al. 2007b), mainly absorb far-red light in vivo. The BChl *b* in purple bacteria has the longest wavelength absorbance (1010 nm) and fluorescence (1050 nm) emissions. However, the detailed characteristics of fluorescence from BChls, such as the fluorescence yield and the variation in light environments, remain poorly understood.

In contrast to the VRE, which tracks the vegetation mass in the remote sensing of the Earth, fluorescence can be used as an indicator of active photosynthesis. The fluorescence signal emitted from the global ground vegetation, which is called solar-induced fluorescence (SIF), can be detected by remote sensing from satellites as the excess light that is seen in the absorption of Fraunhofer lines in sunlight that is reflected from the Earth, which is the apparent increase in the reflectance spectrum due to fluorescence (Maier et al. 2004). The observation of SIF is fundamentally challenging, because the small SIF signal is overwhelmed by large background signals in the reflected sunlight, and high-resolution spectroscopy utilizes specific wavelengths with large solar absorption, which results in the low intensity of the reflected light. The SIF is observed as an infilling effect at these wavelengths. This methodology works because a large contrast is ensured between the Sun and the reflected light from the Earth at specific wavelengths. Thus, SIF has been observed in absorption bands by the Fourier high-dispersion spectrometers on board many environmental satellites (e.g., GOSAT—Hamazaki et al. 2005; Lee et al. 2013; GOME-2—Callies et al. 2000; and GOSAT-2—Nakajima et al. 2012), which have produced a time-series SIF map of Earth (Frankenberg et al. 2014; Sun et al. 2018). We can extract information on the ground vegetation and atmospheric/surface environment, especially the gross primary production, from the changes in the fluorescence map, by calibrating the remote observations with the results of local ground observations (Sun et al. 2018). As with the SIF in Earth observations, the detection of photosynthetic fluorescence on a planet around stars will allow the surface environment and vegetation conditions on exoplanets to be investigated. High-resolution spectroscopy would be necessary for exofluorescence detection, and the contrast between a planet and its host star should be high enough at specific wavelengths. Biofluorescence, similar to that shown by coral reefs on Earth, has been suggested as a new potential biosignature for exoplanets experiencing strong UV radiation from F stars (O'Malley-James & Kaltenegger 2018) and M stars (O'Malley-James & Kaltenegger 2019). This might work if the fluorescence were emitted very efficiently, according to the photons that are gained in the habitats of the exoplanets. As mentioned above, photosynthetic pigments are a potential emitter of biofluorescence. However, neither the yield nor the detectability of photosynthetic fluorescence on the surfaces of exoplanets have yet been examined.

Finding surface biosignatures on Earthlike exoplanets, including the potential detectability of biofluorescence, will be one of the important goals of future astronomy, and it may become possible with future space missions, such as the Large UV/Optical/IR Surveyor (LUVOIR) or the Habitable Exoplanet Observatory, as well as the extremely large next-generation ground-based telescopes (Thirty Meter Telescope,

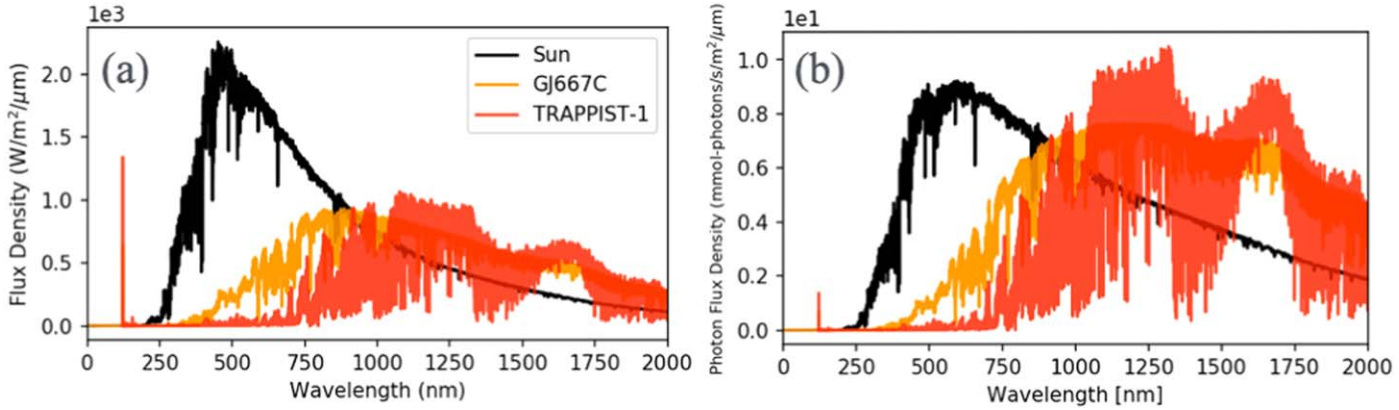

Figure 1. Incident radiation (a) and photon flux density (b) at the TOA of an Earthlike planet around the Sun, GJ667C, and TRAPPIST-1. The spectral data of the Sun, GJ667C, and TRAPPIST-1 were obtained from Meftah et al. (2018), France et al. (2016), and Lincowski et al. (2018), respectively.

Extremely Large Telescope, and Giant Magellan Telescope), observing in reflected light. Thus, it is important to quantitatively evaluate the detectability of any potential surface biosignature by using the expected specifications of specific future missions.

This study constitutes the first attempt at investigating the detectability of photosynthetic fluorescence on Earthlike exoplanets. The remainder of this paper is structured as follows. Section 2 describes the surface vegetation model for an Earthlike planet in the habitable zone (HZ), with the fluorescence emissions being based on the photoresponse of photosynthetic organisms. Section 3 shows the expected fluorescence emissions in the reflected light spectra for an Earthlike planet around an M dwarf or the Sun. In Section 4, we discuss the physiological conditions of photosynthesis that enhance fluorescence emissions, and unique features for future detection, including false-positive signals and seasonal changes. Additionally, we present the detectability of biofluorescence by a future space-based telescope, assuming the LUVOIR telescope parameters, and point out a key spectral feature that will possibly be useful for detections from follow-up observations with high-dispersion spectroscopy. In the final section, we summarize the paper.

2. Materials and Methods

We assume that the radiation from a planetary surface is the sum of the reflected light on the surface and the fluorescence emission from photosynthesis. The outgoing flux on the surface and at the top of atmosphere (TOA) is given by:

$$F^{\uparrow}_{\rm surface}(\lambda) = F^{\downarrow}_{\rm surface}(\lambda)R(\lambda) + F_{\rm fluor.}(\lambda), \quad (1)$$

$$F^{\uparrow}_{\rm TOA}(\lambda) = F^{\uparrow}_{\rm surface}(\lambda)T(\lambda), \quad (2)$$

where λ is the wavelength, $T(\lambda)$ is the atmospheric transmittance (see Section 2.1), $R(\lambda)$ is the surface reflectance of a planet (see Section 2.3), $F^{\uparrow}_{\rm surface}(\lambda)$ is the upward flux from a planetary surface, $F^{\uparrow}_{\rm TOA}(\lambda)$ is the reflected flux at the TOA, and $F_{\rm fluor.}(\lambda)$ is the net fluorescence emission from photosynthesis. $F^{\downarrow}_{\rm surface}(\lambda) = F^{\downarrow}_{\rm TOA}(\lambda)T(\lambda)$ is the downward flux from the planetary atmosphere to the surface, where $F^{\downarrow}_{\rm TOA}$ is the incident flux from a host star at the TOA (see Figure 1 and Section 2.1). In most cases, we neglect the effects of thermal emission and Rayleigh scattering, as both processes contribute little radiation to our spectral region of interest (600–1000 nm).

The transmittance $T(\lambda)$ in the atmosphere of an Earthlike planet through geological evolution was obtained from Rugheimer & Kaltenegger (2018), which was calculated by a 1D coupled radiative/convective–photochemical model for a planetary atmosphere (see also Kasting & Ackerman 1986; Pavlov & Kasting 2002; Segura et al. 2005).

2.1. Stellar Radiation

Two nearby M dwarfs, GJ667 C and TRAPPIST-1, have candidate planets in an HZ. We consider the fluorescence emissions from photosynthesis on an Earthlike planet in HZs around GJ667 C, TRAPPIST-1, and the Sun. We extract the incident stellar flux from high-resolution spectral data for the Sun (Meftah et al. 2018), GJ667 C (France et al. 2016), and TRAPPIST-1 (Lincowski et al. 2018). The incident flux $F^{\downarrow}_{\rm TOA}$ received by Earthlike planets around GJ667 C and TRAPPIST-1 is scaled by the current locations of GJ667C c and TRAPPIST-1e. GJ667 C and TRAPPIST-1 are modeled as M1V and M8V stars. Figure 1 shows the incident flux received by Earthlike planets at the TOAs around the Sun, GJ667 C, and TRAPPIST-1.

2.2. Fluorescence from Photosynthesis

The fluorescence emissions from a planetary surface $F'_{\rm fluor.}$ are expressed as:

$$F'_{\rm fluor.}(\lambda) = sc_v\pi F^{\rm std}_{\rm fluor.} \times f(\lambda), \quad (3)$$

where c_v is the surface coverage of the vegetation (see Section 2.3), s is the scaling factor from the standard observed fluorescence emission reflecting the photosynthetic activity, and $F^{\rm std}_{\rm fluor.}$ is the standard fluorescence intensity from vegetation, based on field measurements. The spectral shape of fluorescence emission from a photosynthetic organism at wavelength λ is defined by $f(\lambda)$. In this study, $F^{\rm std}_{\rm fluor.} = 1.0$ (W m^{-2} μm^{-1} sr^{-1}; Du et al. 2019; Yao et al. 2021) and $s = 0$, 1, 5, and 10. The net fluorescence intensity $F_{\rm fluor.}$ is calculated by considering the photons acquired at the habitat, using $F'_{\rm fluor.}$ in Equation (3):

$$F_{\rm fluor.}(\lambda) = \frac{\chi}{\chi_0}F'_{\rm fluor.}(\lambda), \quad (4)$$

$$\chi \equiv \int n(\lambda)\sigma(\lambda)d\lambda, \quad (5)$$

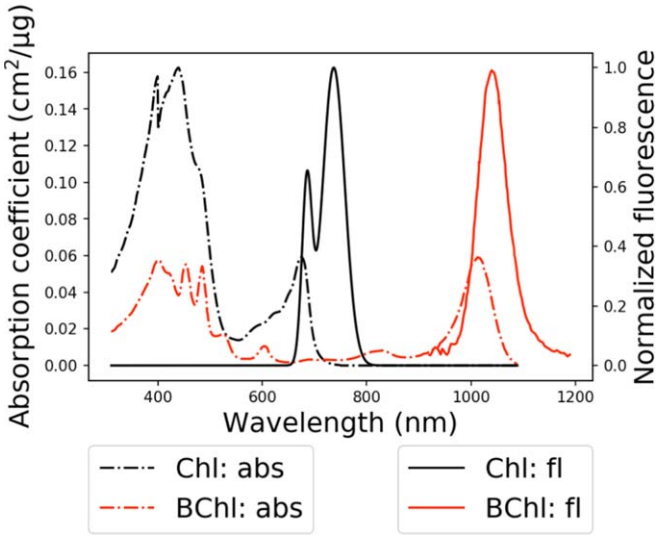

Figure 2. Fluorescence ($f(\lambda)$: solid curves) and photoabsorption ($\sigma(\lambda)$: dashed curves) spectra for Chls (black) and BChls (red). The absorption coefficient of the Chls, in units of $cm^2\ \mu g^{-1}$, was obtained from Feret et al. (2008). The fluorescence spectra are expressed by the Gaussian functions given in Frankenberg et al. (2012) and Guanter et al. (2010). For the BChls, $f(\lambda)$ and $\sigma(\lambda)$ adopt those of the LH1–RC complex of a BChl *b* containing purple photosynthetic bacteria (Magdaong et al. 2016). The nondimensional absorption spectrum for the BChls is normalized at the peak value in the longest absorption band, the *Q* band, of the Chls. The two fluorescence spectra are normalized at their peak values.

$$\chi_0 \equiv \int n_{\mathrm{sun,ref.}}(\lambda)\,\sigma_{\mathrm{chls}}(\lambda)\,d\lambda, \tag{6}$$

where χ is the light absorption efficiency, $n(\lambda)$ is the photon flux density at the planetary surface, and $\sigma(\lambda)$ is the absorption coefficient of a photosynthetic pigment. χ_0 represents the standard absorption efficiency on Earth. The subscript "chls" on $\sigma(\lambda)$ represents Chls (see "Chl: abs" in Figure 2). $n_{\mathrm{Sun,ref.}}(\lambda)$ is the photon flux density on the surface of the Earth, from the reference solar spectral irradiance at an air mass of 1.5 (National Renewable Energy Laboratory), which corresponds to a typical irradiance for Earth vegetation.

We consider an incident flux from a star under two sky conditions—a clear sky and 60% cloud cover—to estimate the reflectance at the TOA and the χ on the ground, in accordance with the setup of the simulation. We assume the clear sky condition, unless specified otherwise, with the cloudy condition only appearing in Section 4.3.1 (Figure 12). In the cloudy condition, 60% of the radiation is reflected in three kinds of clouds, and 40% of the radiation reaches the ground. For the clouds, we assume that 40% are low-water clouds, 40% are high-water clouds, and 20% are high-ice clouds (Gao & Kaufman 2003) at altitudes of 1, 6, and 12 km, respectively. To model Earthlike conditions, the effect of Rayleigh scattering in the planetary atmosphere was also considered in the cloudy condition, using an empirical approach, as previously described by Bucholtz (1995; see Appendix A for more details).

Equation (4) indicates that $F'_{\mathrm{fluor.}}$ is linearly scaled to the number of incoming photons that are absorbed by Chls at the planetary surface. In other words, Chls can emit strong fluorescence if the spectral shapes of $n(\lambda)$ and $\sigma(\lambda)$ match well. Note that $n(\lambda)$ is exactly the same as $F^{\downarrow}_{\mathrm{surface}}(\lambda)$, and its unit is shown in Figure 1(b) ($F^{\downarrow}_{\mathrm{TOA}}$ in the figure). This treatment in Equations (3) and (4) can be applied to the relationship between the incoming photons and the photons emitted as fluorescence on an Earthlike planet around various stars other than the Sun.

Figure 2 shows the normalized spectra of the fluorescence $f(\lambda)$ and the absorption coefficient $\sigma(\lambda)$ for Chls and BChls. The peak wavelength of $f(\lambda)$ is redshifted from that of $\sigma(\lambda)$, which is called the Stokes shift (Lakowicz 2006). There are two absorption bands in the $\sigma(\lambda)$ of the Chls: the *B* band (known as the Soret band) in the short-wavelength region and the *Q* band in the long-wavelength region. The primary fluorescence emission is derived from the *Q* absorption band. In this study, we model $f(\lambda)$ for the Chls as the superposition of two Gaussian distributions (Guanter et al. 2010; Frankenberg et al. 2012), with means of 680 nm (PSII) and 740 nm (PSI and PSII). $\sigma(\lambda)$ for the Chls uses the model vegetation with Chls ($\sigma_{\mathrm{chls}}(\lambda)$) (Feret et al. 2008). We obtained $f(\lambda)$ and $\sigma(\lambda)$ for the BChls from the spectral data for the LH1–RC complex, the supramolecular complex of the light-harvesting core antenna (LH1) and the RC in a BChl *b* containing purple photosynthetic bacteria (see Figure 3 in Magdaong et al. 2016). Note that we only use $\sigma(\lambda)$ in the *Q* band to calculate χ and χ_0 because the free Chls and BChl–protein complexes in each solution affect each spectrum in the *B* band to different degrees.

2.3. Surface Vegetation

To determine the detectability of the vegetation fluorescence, we use two leaf models for our experiments: one that assumes the reflectance spectrum and fluorescence of standard Chl and another that uses a scaled version of the spectrum of BChl. The reflectance of a planet is expressed as $R(\lambda) = \sum_i c_i r_i(\lambda)$, where *i* denotes the surface type, c_i is the fraction of surface coverage of type *i*, and r_i is the reflectance of type *i*. We obtain the reflection spectra for various surface types—including vegetation, oceans, and coasts—from the USGS Digital Spectral Library and the ASTER Spectral Library (Baldridge et al. 2009). The detailed compositions used in this paper are summarized in Table 1. The reflectance of the surface vegetation r_v is estimated from radiation transfer calculations for a modeled leaf (Jacquemoud & Baret 1990; Feret et al. 2008), using $\sigma(\lambda)$ over all the wavelengths shown in Figure 2. Figure 3 shows the reflectance of a Chl-based leaf ("standard") and a BChl-based leaf ("hypothetical"). In the latter case, we assume that vegetation on a different planet has a photosynthetic pigment whose optical property is the same as that of BChl, exhibiting the VRE in the longer-wavelength region, as shown in Figure 3. As the input to the radiation transfer calculations, we use the absorption spectra of Chl (Feret et al. 2008) and BChl (Magdaong et al. 2016). The unitless absorption spectrum for BChl is normalized at the peak of that for Chl, unlike the calculations of χ and χ_0 in Section 2.2. As shown in Figure 3, both Chl- and BChl-based leaves show a large reflectance (i.e., the VRE) in the wavelength ranges around 700–750 and 1000–1100 nm. The green bump around 500 nm is observed in the reflectance for Chl, and larger and broader bumps are observed from ~500 to 950 nm for BChl, from the larger difference in wavelength between the *B* and *Q* bands, than are observed for Chl. As with many kinds of photosynthetic organisms, the organisms with BChl could have acquired accessory pigments, such as carotenoids, which absorb photons with wavelengths between the *B* and *Q* bands of Chl (Cogdell 1978). The effective light absorption by accessory pigments can suppress the increase in the reflectance.

Table 1
The Surface Composition, Vegetation, Fluorescence Type, and Atmospheric Transmittance ($T(\lambda)$) for All the Cases in This Paper

Model Name	Surface Composition	Surface Vegetation	Fluorescence Type	$T(\lambda)$	c_v
veg-only 0C	100% vegetation	Chl surf.	Chl fluor.	0.0 Ga	1.00
veg-only 2C				2.0 Ga	
veg-only 0B		BChl surf.	BChl fluor.	0.0 Ga	
veg-only 2B				2.0 Ga	
veg-land 0C	70% ocean, 2% coast, and 28% vegetation	Chl surf.	Chl fluor.	0.0 Ga	0.28
veg-land 2C				2.0 Ga	
veg-land 0B		BChl surf.	BChl fluor.	0.0 Ga	
veg-land 2B				2.0 Ga	
mod-earth 0C	70% ocean, 2% coast, and 28% mixed land (with 16.8% vegetation)	Chl surf.	Chl fluor.	0.0 Ga	0.168
mod-earth 2C				2.0 Ga	
mod-earth 0B		BChl surf.	BChl fluor.	0.0 Ga	
mod-earth 2B				2.0 Ga	
anoxic B	70% ocean, 2% coast, and 28% mixed land at 3.9 Ga	⋯	BChl fluor.	3.9 Ga	0.72

Note. "Mixed land" is composed of 60% vegetation (16.8% in total), 15% snow, 9% granite, 9% basalt, and 7% sand (Baldridge et al. 2009); "mixed land at 3.9 Ga" means the land model of the Archean Earth at 3.9 Ga, which is composed of 40% granite, 35% basalt, 15% snow, and 10% sand. "Chl surf." and "BChl surf." correspond to the reflection spectra of Chl and BChl in Figure 3, respectively. The spectral shapes of the fluorescence emissions $f(\lambda)$ for "Chl fluor." and "BChl fluor." correspond to the fluorescence spectra of Chl and BChl in Figure 2, respectively; their intensities $F_{\text{flour.}}$ are scaled in Equations (3) and (4). c_v is given by the relationship between the surface coverage of the vegetation and the fluorescence emission. $s = \{0, 1.0, 5.0, 10.0\}$. We obtain $T(\lambda)$ at 0.0, 2.0, and 3.9 Ga from Rugheimer & Kaltenegger (2018).

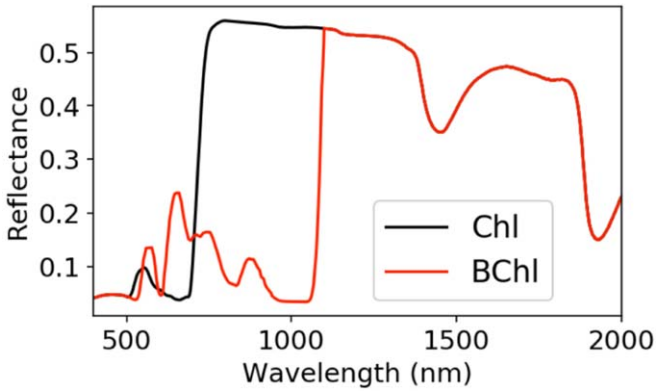

Figure 3. The reflectance of the vegetation estimated from radiation transfer calculations for two leaf models: Chl ("standard") and BChl ("hypothetical"; Jacquemoud & Baret 1990; Feret et al. 2008). The light absorption spectra for Chls and BChls use $\sigma(\lambda)$ from Figure 2.

With or without accessory pigments, the bump for BChl does not affect the fluorescence emissions in the wavelength (see Figures 7, 8, and 10). The low reflectance from ∼500 to 700 nm (1000 nm), due to the light absorption by Chls (BChls), affects the reflectance of the planet. The degree of reduction in the overall planetary reflectance varies, depending on the surface coverage by the vegetation.

3. Results

We considered three fluorescence cases on an Earthlike planet at different stages of atmospheric evolution around the Sun, GJ667 C, and TRAPPIST-1, with different surface biosignatures: Earthlike (Chl-based) vegetation, hypothetical BChl-based vegetation, and biological fluorescence without any surface vegetation. Our models for the surface composition, vegetation, fluorescence type, and atmospheric composition, i.e., transmittance, are summarized in Table 1. "Mod-earth" corresponds to the surface condition for the Modern Earth, leading to a lesser contribution of fluorescence emissions than in the other two cases. The "veg-only" models are considered optimistic conditions for fluorescence emissions, where vegetation covers the whole planetary surface. The "veg-land" models, with 70% ocean, 2% coast, and 28% land covered with the vegetation, lie between the mod-earth and veg-only models. As mentioned in Section 2, we consider two leaf models for land vegetation: Chl-based vegetation and BChl-based vegetation. For the atmospheric compositions of an Earthlike planet, we adopt the Modern Earth model at 0.0 Ga (oxygen-rich atmosphere), the Paleoproterozoic Earth model at 2.0 Ga (oxygen-poor atmosphere), and the Archean Earth model at 3.9 Ga (anoxic atmosphere; see Table 1 in Rugheimer & Kaltenegger 2018). As an extreme case, we assume the presence of photosynthetic bacteria with BChl spread over the land and ocean on an Archean Earth–like planet with no surface vegetation. We assume a clear sky for all the atmospheric conditions in Section 3.

3.1. Case 1: Planets with Earthlike Vegetation

In case 1, Earthlike vegetation (Chl) emits fluorescence on the surface of an Earthlike planet. The fluorescence emissions from Chl are visible at wavelengths from 650 to 800 nm, as shown in Figure 2. To determine the contribution of the fluorescence from the planets, the reflectance is defined as $F^{\uparrow}_{\text{TOA}}(\lambda)/F^{\downarrow}_{\text{TOA}}(\lambda)$ and calculated. Figures 4 and 5 show the reflectance of an Earthlike planet with Modern Earth's atmosphere (0.0 Ga) and an oxygen-poor atmosphere (2.0 Ga), respectively. The O_2, O_3, CH_4, and H_2O absorption features in the atmosphere are imprinted in the reflectivity in the visible–NIR wavelengths from 600 to 800 nm. The oxygen-poor atmosphere models show less conspicuous patterns in the reflectance profile in the 700–750 nm wavelength region. The reflectivity between 600 and 700 nm is nearly constant, but it increases with the decreasing surface coverage of the vegetation. The VRE is observed as a steep rise in the

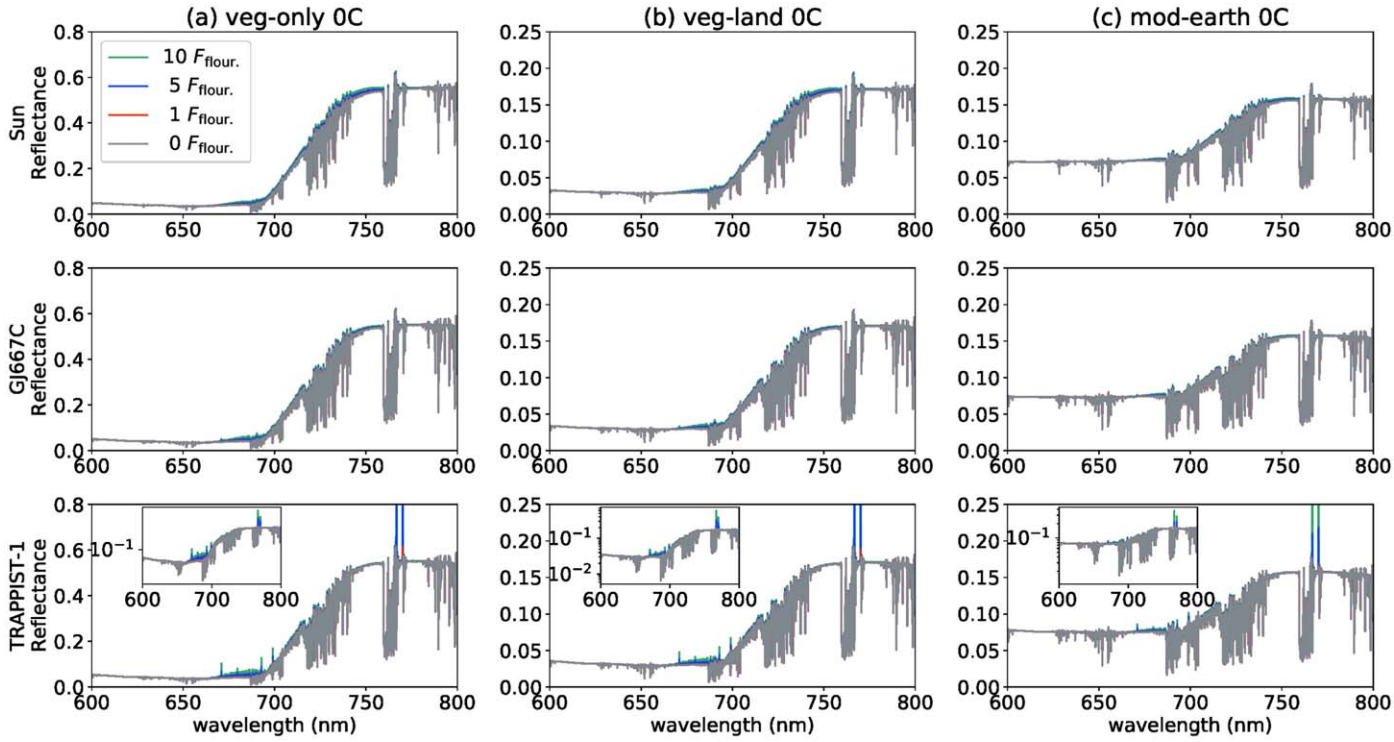

Figure 4. The reflectance of an Earthlike planet with the Modern Earth's atmosphere (0.0 Ga) around the Sun, GJ667C, and TRAPPIST-1. The three colors represent the reflected light from a planet with $F_{\rm fluor.}$ ($s = 1$: red), $5F_{\rm fluor.}$ ($s = 5$: blue), and $10F_{\rm fluor.}$ ($s = 10$: green), where $F_{\rm fluor.}$ is the fluorescence emission from Chls observed on the Earth. Models with no fluorescence emission are also indicated by the gray lines. We assume that Earthlike vegetation (Chl) covers the planetary surface (see Table 1 for the model details). The reflectance is defined here as $F^{\uparrow}_{\rm TOA}(\lambda)/F^{\downarrow}_{\rm TOA}(\lambda)$, where $F^{\uparrow}_{\rm TOA}(\lambda)$ is the light reflected from the ground at the TOA and $F^{\downarrow}_{\rm TOA}(\lambda)$ is the flux at the TOA induced by stars. For each case around TRAPPIST-1, the reflectance with a logarithmic scale is shown as the inset plot.

reflectance from 700 to 750 nm (see also Figure 3), whereas the reflectance excess due to fluorescence is quite small, even in optimistic conditions (veg-only models). Note that the red curve with $1F_{\rm fluor.}$ around the Sun in the mod-earth model (Figure 4), corresponding to the Modern Earth fluorescence, is hardly seen. Around TRAPPIST-1, however, the sharp increase in the reflectance around 770 nm is due to the strong absorption of potassium in the stellar atmosphere. As a result, we observed similar features in the light reflected from an Earthlike planet with different atmospheric compositions around TRAPPIST-1 (see Section 4.3.2 for further discussion).

Figure 6 shows the reflectance excess due to fluorescence emissions on an Earthlike planet with the Modern Earth's atmosphere. Atmospheric absorptions—such as H_2O, O_2, and O_3—weaken the Gaussian features in the fluorescence emissions from an Earthlike planet around the Sun. The fluorescence from Chls around 740 nm is less pronounced for a planet around M dwarfs than for one around the Sun because of the weaker radiation flux in the wavelength region 700–750 nm (see Figure 1). In addition, a sudden increase in reflectance due to the VRE obscures the fluorescence emission around 740 nm (see Figures 4 and 5). As a result, the Chl fluorescence around 680 nm emitted from PSII on an Earthlike planet would be the most promising feature for detection (see Figure 2). Note that nonphotochemical quenching processes can decrease the fluorescence intensity around 680 nm, and the fluorescence emission is further reduced by the reabsorption of photons within the canopy (Porcar-Castell et al. 2021).

3.2. Case 2: Planets with BChl-based Vegetation

In case 2, BChl-based vegetation, as the major photosynthetic pigment, covers the surface of a planet. The BChls are assumed to emit the same degree of fluorescence intensity as the Earth's vegetation. As shown in Figure 2, fluorescence from BChls occurs in the wavelength range from 1000 to 1100 nm. In contrast to case 1, fluorescence emissions with 5 and $10F_{\rm fluor.}$ show strong features around 1050 nm in almost all conditions, as shown in Figures 7 and 8. Identifying the fluorescence at the Earth's vegetation level ($\lesssim F_{\rm fluor.}$) remains challenging even in the optimistic case—that is, (a) veg-only 0B. The reflectivity between 1000 and 1050 nm becomes slightly higher for mod-earth models with less surface vegetation coverage. As shown in Figure 9, the BChl organisms absorb photons efficiently and emit fluorescence with less absorption and scattering in the planetary atmosphere. We assume that the fluorescence emissions from BChls are invulnerable to blending with the steep increase in the reflectance by the VRE. As a result, we find a more significant fluorescence contribution to the reflected light in case 2.

Atmospheric properties—such as chemical compositions and cloud coverage—change the fluorescence profile. The water absorption is weak for wavelengths from 1000 to 1100 nm. If the major absorption bands of a photosynthetic pigment lie in wavelengths longer or shorter than 1000–1100 nm, the presence of water vapor in the atmosphere complicates the detection of fluorescence emissions. Strong absorption due to CH_4 in an oxygen-poor atmosphere also hides fluorescence near 1000 nm (see the GJ667C models in Figure 8). The BChl

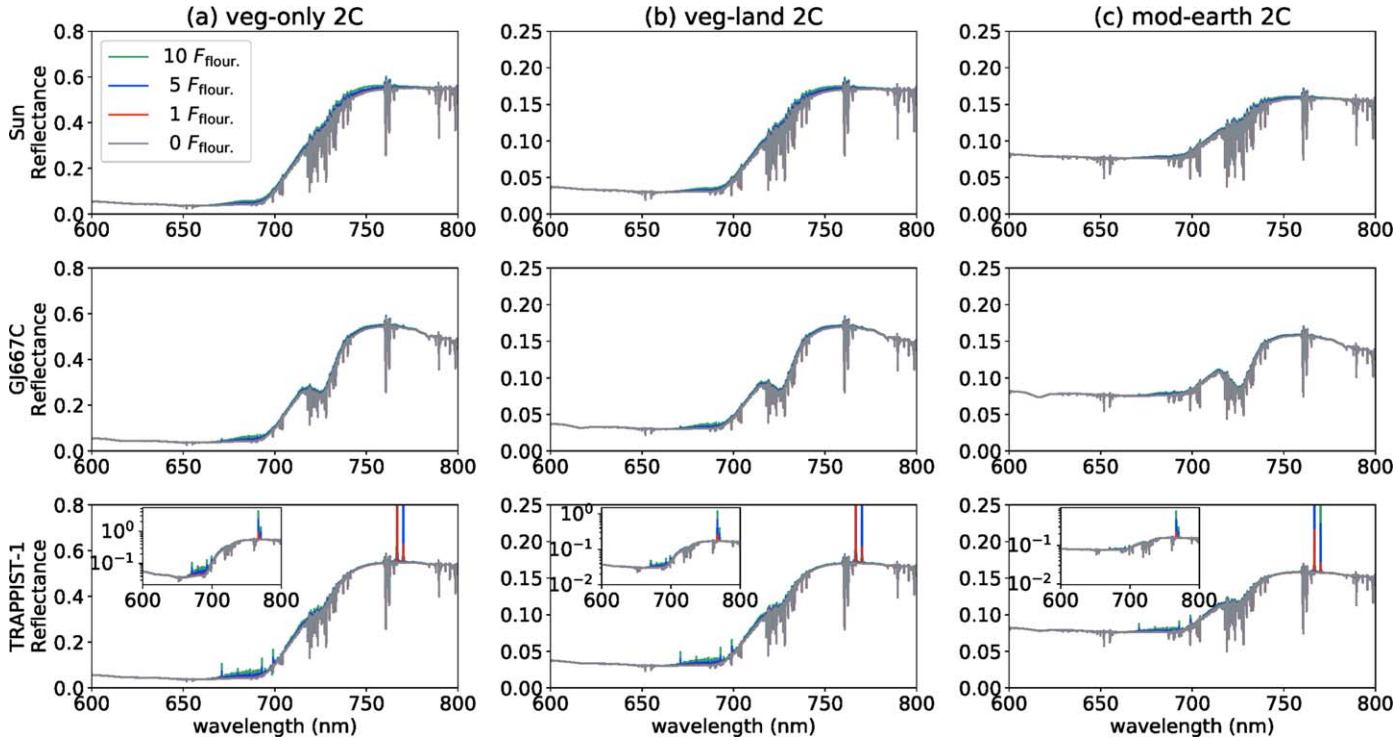

Figure 5. The same as Figure 4, but for an Earthlike planet with an oxygen-poor atmosphere (2.0 Ga).

organisms bearing BChl *b* and the Stokes shift are ideal for detecting fluorescence at wavelengths longer than the characteristic wavelength of the fluorescence from Chls. Thus, fluorescence in the wavelength range of 1000–1100 nm could be a suitable biosignature for photosynthetic organisms—such as BChls—on planetary surfaces, unless they coexist with strong absorbers near 1000 nm.

The VRE with a sharp rise in the reflectance is observed in the wavelength range from 1050 to 1100 nm in case 2, as shown in Figure 3. The reflectance excess due to BChl fluorescence is 0.01–0.05 for the Modern Earth atmosphere models (see Figure 9), whereas that due to the VRE is 0.4–0.5 (0.1–0.15) for the veg-only models (the veg-land and mod-earth models). The BChl fluorescence causes a slight increase in the reflectance around 1000–1100 nm compared to the VRE. Such a nonprominent fluorescence emission with a Gaussian shape at a wavelength different from the VRE feature can be extracted from the reflectance profile using data processing, such as principal component analysis. Photosynthetic organisms different from those around the Sun are expected to exhibit VRE and fluorescence features at different wavelengths. Thus, not only spectral features that are due to atmospheric molecules, but also the simultaneous detection of the VRE and fluorescence will help to identify traces of photosynthesis on an exoplanet. When we find a possible signal of the VRE, the fluorescence could potentially be useful for further validation, because the VRE signal is stronger than the fluorescence one.

3.3. Case 3: Anoxic World (without VRE)

In case 3, an Earthlike planet has the same reduced atmosphere as the Archean Earth at 3.9 Ga. Anoxic bacteria with photosynthetic pigments, such as BChls, may spread over the surface of a planet with a CO_2-rich atmosphere. Anoxic bacteria are assumed to live in the ocean and on the coast (i.e., $c_v = 0.72$), and only to emit fluorescence with an intensity that is comparable to the standard emission from land plants, without the distinct reflectance of a vegetation surface. The fluorescence emissions from anoxic bacteria adopt those from BChls on the Earth. Figure 10 shows the reflectance of an Archean Earth–like planet with BChl-based bacteria. In the reflection spectra, strong water absorption appears around 950 and 1150 nm. The relatively high reflectance across the wavelength range is mainly from the light reflected by the land. We observe fluorescence emissions in the wavelength range between 1000 and 1100 nm, owing to the lack of light reflected from BChl-bearing oceanic bacteria, including the VRE feature. The intense absorption in the stellar atmosphere enhances the apparent reflectance of a planet around TRAPPIST-1 (see also Figures 4 and 5, as well as Section 4.3.2).

4. Discussion

This study demonstrates the reflectance with photosynthetic fluorescence on an Earthlike planet around the Sun and two M dwarfs. This section reviews the biological processes of photosynthesis, then considers the future detection of biofluorescence on an exoplanet. In Section 4.1, we discuss the possible physiological conditions that could enhance the fluorescence emissions on a planet, based on our understanding of Chl fluorescence. In Section 4.2, we discuss possible false-positive or negative detections of fluorescence (Section 4.2.1), as well as the potential usage of the nonlinear photoresponse of the fluorescence yield to the excitation light intensity to distinguish between biofluorescence and the false-positive/negative signals of fluorescence (Section 4.2.2). Finally, in Section 4.3, we show the fluorescence detection with telescopes. We present the detectability of the fluorescence

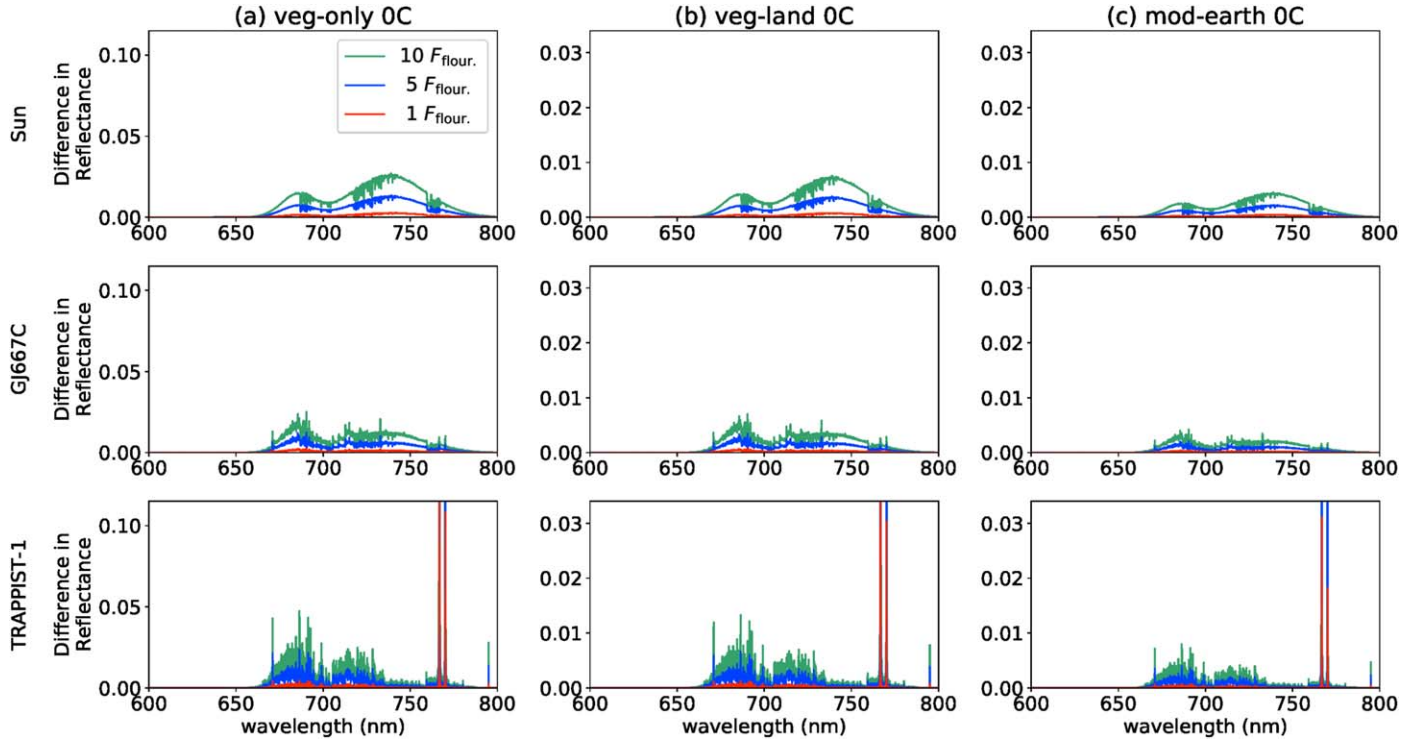

Figure 6. The reflectance excess due to Chl fluorescence emissions on an Earthlike planet with the Modern Earth's atmosphere.

from an Earth twin around a Sunlike star using the noise model for a LUVOIR-A-like mission (Section 4.3.1), and the remarkable enhancement in the reflectance due to the absorption lines of stars, which could be a promising feature for detection by high-dispersion spectroscopy, especially around ultracool stars (Section 4.3.2).

4.1. Possible Physiological Conditions Supporting Fluorescence Detection

This study has adopted the typical fluorescence spectrum of Chl-containing plants and LH1–RC purified from BChl *b*–bearing purple bacteria. The fluorescence spectrum of the LH1–RC complex suspended in buffer solution was measured under laboratory conditions, with a low concentration of LH1–RC in the solution, to avoid the reabsorption of fluorescence. Cells having LH1–RC in vivo would result in a ∼50 nm shift in the spectral peak wavelength toward longer wavelengths under dense conditions, because the reabsorption of the fluorescence reduces the shorter-wavelength fluorescence. A redshifted fluorescence spectrum should still be observable, because it is located within the atmospheric window. For the fluorescence intensity of vascular plants on the ground, we refer to the standard value ($F_{\rm fluor.}$) of the fluorescence model for exoplanets in our simulations. The possible detection of fluorescence emissions on exoplanets would require $\gtrsim 5F_{\rm fluor.}$ with BChl (see Figures 7, 8, and 10). There are four potential factors that could increase the fluorescence yield in photosynthetic organisms, from the biophysical viewpoint of photosynthetic studies on existing phototrophs on the Earth.

1. Increasing the Chl/BChl concentration per the land area. High concentrations of Chls and BChls enhance their fluorescence intensity. In general, the Chl/BChl concentration in a cell increases to capture as many photons as possible under low-light conditions. The fluorescence increases linearly with the Chl/BChl concentration when the cell density is low. In contrast, the fluorescence intensity reaches a saturation level in highly dense environments, due to the reabsorption of the fluorescence by cells (Du et al. 2017).
2. A small spectral overlap between absorption and fluorescence. The large separation between the main absorption band and the fluorescence band increases the fluorescence intensity of concentrated cells. In photosynthetic organisms, the excitation energy is transferred between Chls, and the Chl fluorescence tends to be emitted from long-wavelength Chls (LWCs), which have the reddest absorption band in a photosystem, because the excess excitation energy is easily trapped at the lowest energy level. A redshift in the peak wavelength of the fluorescence and a blueshift in the absorption, which can be caused by the modification of the vibronic interactions of pigments between surrounding the proteins and solvent, can reduce the spectral overlap between the fluorescence and the absorption. In some conditions, the fluorescence emission from the LWCs is redshifted by more than 50 nm from that of the bulk Chls. Although most plants have a small amount of LWCs in PSII, and the Chl fluorescence is absorbed well in high-Chl concentrations, far-red absorbable LWCs contributing to PSII have been reported in some eukaryote algae (Fujita & Ohki 2004; Wilhelm & Jakob 2006; Kotabová et al. 2014; Wolf et al. 2018; Kosugi et al. 2020). These algae show a significant fluorescence emission at far-red light wavelengths (700–800 nm) at room temperature, and some of them decrease the overlap (Fujita & Ohki 2004; Kosugi et al. 2020).
3. Low photosynthetic efficiency. The photon loss in photosynthetic processes reduces the photon yield of

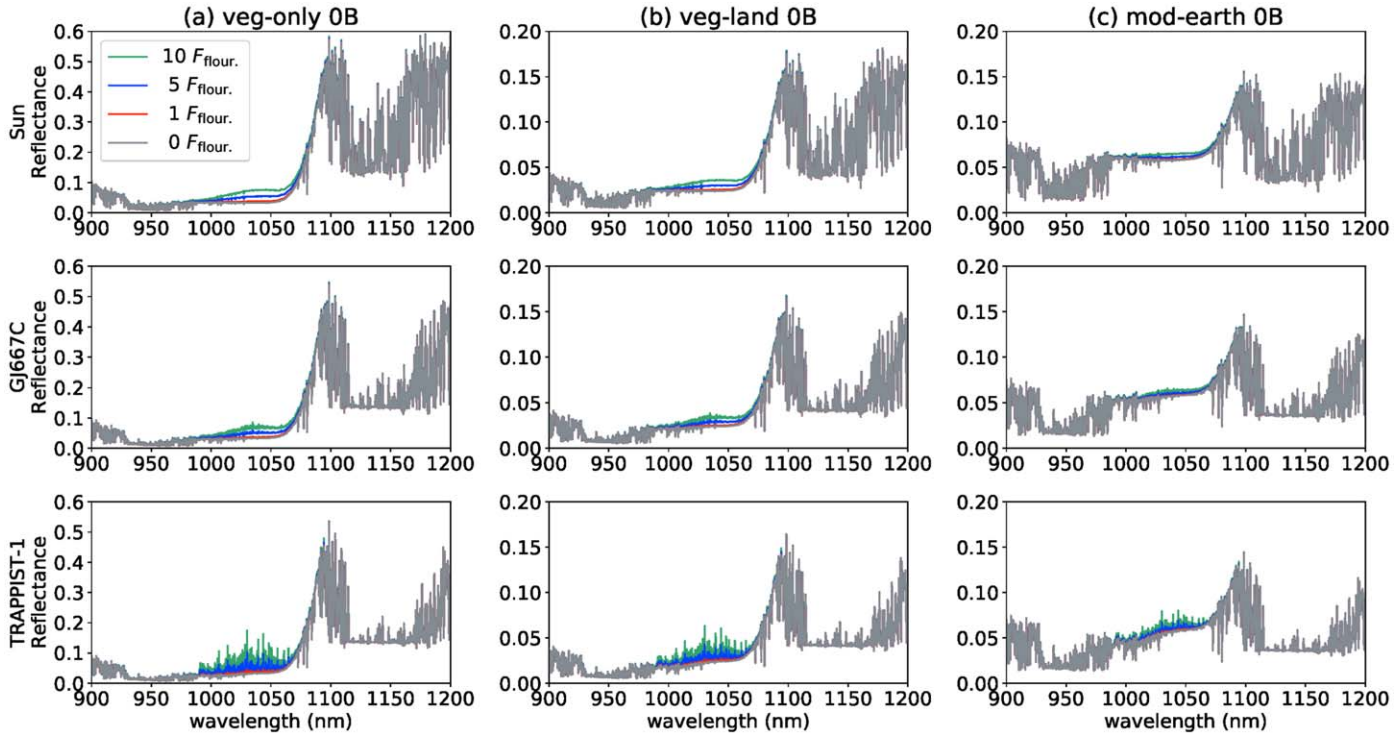

Figure 7. The same as Figure 4, but for the reflectance of a planet covered with BChl-based vegetation.

the fluorescence. The excitation yield in PSII has increased throughout the evolutionary processes of photosystems. For example, the increase in the light use efficiency in oxygenic photosynthesis on Earth has been achieved by the light-harvesting antenna protein from the membrane of superficial phycobilisome in cyanobacteria changing to the light-harvesting Chl-binding protein in eukaryotic algae. Furthermore, the subsequent modifications of LHCs have achieved higher photosynthetic quantum yields in the evolution process. The maximum excitation yield in PSII of vascular plants is estimated to be ∼0.9, whereas those of green algae and cyanobacteria are ∼0.8 and ∼0.6, respectively (Schuurmans et al. 2015). Suppose that phototrophs on an exoplanet are in an early stage of evolution. In such a case, the expected fluorescence yield may be high, to compensate for the low efficiency of the photon yields in primitive photosynthesis.

4. Suppression of heat dissipation. Photon loss due to heat dissipation in photosynthetic pigments suppresses the photon yield of the fluorescence. Heat dissipation occurs in the vibrational relaxation of excited pigment molecules, Chls, or accessory pigments, such as carotenoids. Additionally, light-dependent protection mechanisms for dissipating the excess light energy as heat are inherent in all the cyanobacteria, algae, and plants. The efficiency of the heat dissipation largely depends on the molecular configuration and the environments of pigments binding to proteins. The energy conversion rate from light to heat in photosystems is crucial in estimating the photosynthetic fluorescence on other planets.

Therefore, the fluorescence yields of photosynthetic pigments should fluctuate over time, due to photosynthetic activity and heat dissipation.

4.2. Further Identifications for Confirming Photosynthetic Fluorescence

4.2.1. Potential False Positives/Negatives of Biological Fluorescence Detection from Exoplanets

The photosynthetic pigments on an exoplanet may be different from those on Earth, and the relevant wavelengths for fluorescence emission from exovegetation continue to be unknown. A possible fluorescence signal on another planet could be a false-positive or false-negative detection of biological activities. The main sources potentially causing false-positive/false-negative detections could be surface reflectance or fluorescence from the minerals on the exoplanets. In our study, both Chl and BChl fluorescence can be contaminated by mineral fluorescence, but it is not plausible to expect the fluorescent minerals to cover a fraction of a planetary surface comparable to Earth's vegetation, given our knowledge of the Earth's environment. Recently, solar-induced mineral luminescence has been extracted from SIF data obtained by remote sensing of the Earth (Köhler et al. 2021). This study revealed that about 10% of nonvegetated areas are weakly luminescent, and it speculated that the luminescence came from some spots that were covered by carbonate with Mn^{2+} and was comparable to SIF (or Chl fluorescence). However, those areas are negligible on the planetary scale. On the other hand, mineral fluorescence could pollute, to an extent, fluorescence in the NIR, including the BChl fluorescence. For instance, silicate (e.g., pyroxene and olivine) shows a prominent absorption around 1000 nm caused by Fe^{2+} (Sunshine & Pieters 1998; Klima et al. 2011; Bishop et al. 2019). Its fluorescence could appear at a slightly longer wavelength from the absorption, with an energy corresponding to the Stokes shift, like other NIR fluorescent materials (Selvaggio et al. 2020; Jackson et al. 2021). While

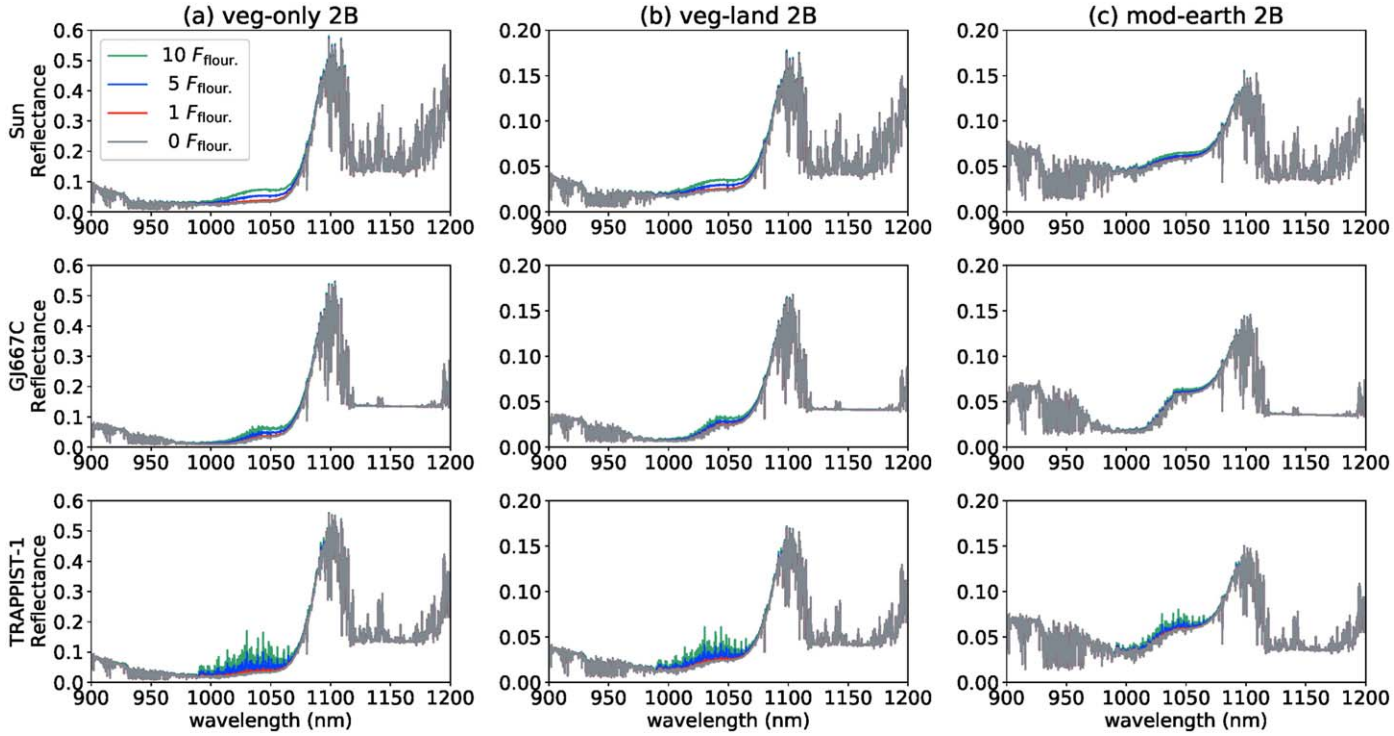

Figure 8. The same as Figure 7, but for a planet with an oxygen-poor atmosphere (2.0 Ga).

there are a variety of fluorescent minerals (e.g., fluorite, calcite, and corundum), we do not deny the possibility that unexpectedly strong mineral fluorescence could be observed on exotic planets, such as a carbide exoplanet (Allen-Sutter et al. 2020) whose surface could be covered by diamond with lattice defects, e.g., due to a nitrogen-vacancy center (Schirhagl et al. 2014). Characterizing atmospheric features is helpful for understanding the potential fluorescence features of the surface components of an exoplanet, e.g., rocks and minerals. Besides, as already mentioned, the simultaneous detection of vegetation reflectance (VRE) and fluorescence features could help to identify photosynthesis.

4.2.2. Nonlinear Photoresponse in Photosynthesis

Photosynthetic organisms regulate metabolic processes to maximize the use of available photons under light conditions and emit biological fluorescence by converting light energy via photochemical reactions. The nonlinear response of the fluorescence yield to the excitation light intensity would be a clue for finding the presence of photosynthetic organisms. If a planet is in an elliptical orbit, the incident flux received by the planet from its host star varies over time. The fluorescence emissions from nonbiological processes increase with the incident light intensity. In contrast, the saturation level of the fluorescence intensity from biological activities, such as photosynthesis, exists because the quantum yields of Chl fluorescence vary according to the light environment and atmospheric CO_2 concentrations. The quantum yields of Chl fluorescence are primarily involved in the reduction states of the electron acceptors of photosystems for electron transports and the excitation energy quenching by photoprotection mechanisms (see Genty et al. 1989; Krause & Weis 1991; Baker 2008). A sudden intense light can induce a reduction in the electron acceptors of PSII, where the oxidation of water to generate O_2 occurs as a primary step in photosynthesis. The presence of photoprotection mechanisms also modulates the quantum yields of Chl fluorescence. When dark- or dim-light-adapted leaves are suddenly irradiated with intense light, the Chl fluorescence quantum yields rapidly increase, by up to five times. Accordingly, the relationship between the fluorescence yield and the excitation light intensity (i.e., the number of absorbed photons) provides a hint for exploring the origin of fluorescence on a planet.

4.3. Detectability of Biological Fluorescence by Future Telescopes

4.3.1. The Earth–Sun System as an Earth Twin in a LUVOIR-A-like Mission

We investigate the detectability of the fluorescence from an Earth twin around a Sunlike star at 10 pc from the Earth, assuming a LUVOIR-A-like space telescope. Figure 11 presents the simulated spectra of a second Earth around a Sunlike star at 10 pc, with the biological fluorescence. We apply the noise model used in Robinson et al. (2016) and Kopparapu et al. (2021), which accounts for planet photons, stellar photon noise, and background noise, e.g., zodi, exozodi, readout, and dark current noises, with the throughput assuming the LUVOIR-A telescope. The parameters and the formalism used in this paper are presented in Appendix B. Figures 11(a)–(c) show the results of the most optimistic model for the fluorescence signal (veg-only 0B) from the Earth–Sun system observed from 10 pc with a 15 m space telescope. The original data are the same as those for the Sun in Figure 7(a). In Figure 11(a), the F_p/F_s observed by the telescope for each wavelength bin are shown as the solid lines, with the random noise displayed as the 1σ error bars for each bin, over 9000 hr of exposure time, where F_p is the reflected light from the planet and F_s is the starlight. Figure 11(b) depicts a magnification of

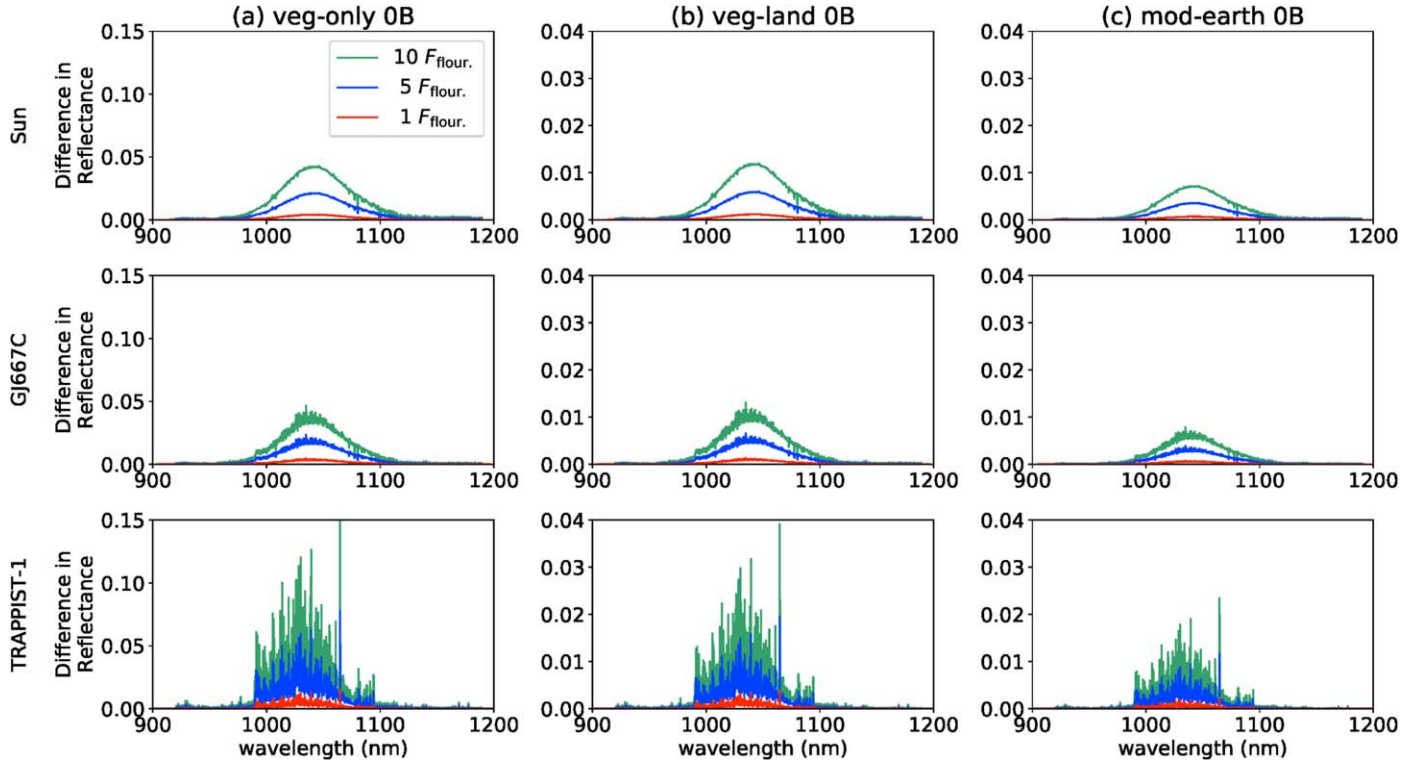

Figure 9. The reflectance excess due to BChl fluorescence emissions on an Earthlike planet with the Modern Earth's atmosphere.

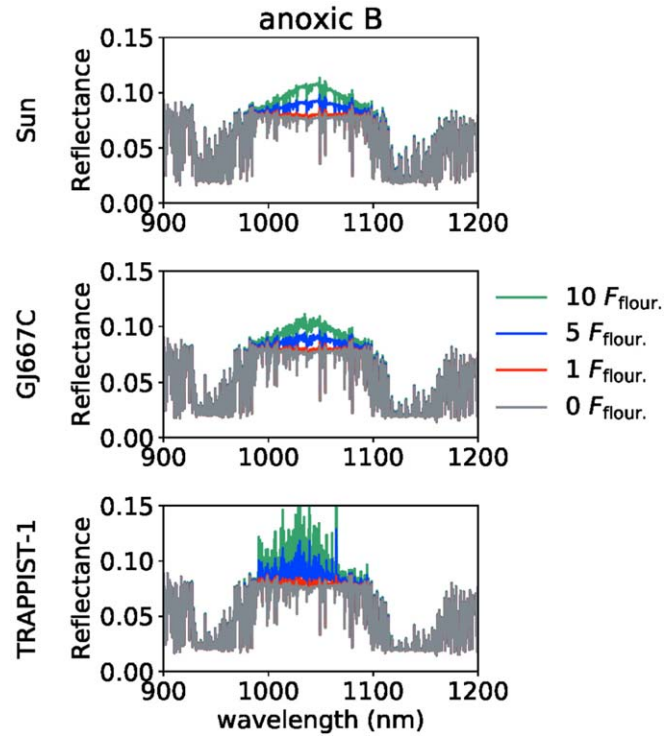

Figure 10. The reflectance of an Earthlike planet with an anoxic atmosphere and no land vegetation (anoxic B).

the spectrum in Figure 11(a). Some of the error bars are beyond the solid lines, but the spectral features of the fluorescence emissions are recognizable for each case in the figure. Figure 11(c) shows the signal-to-noise ratio (S/N), with the same observation time as in Figure 11(a). The difference between 0 and 5 $F_{\rm fluor.}$ is larger than 1σ. To detect the fluorescence with a 3σ error, ∼50,000 hr of exposure time are required, and with a 5σ error, ∼100,000 hr, or 10 yr, are expected (not shown in the figures). Thus, years or observations would be required for fluorescence detection, even by a LUVOIR-A-like space telescope, meaning that it would be extremely challenging to observe one target. In less optimistic models, namely, the veg-land 0B model around the Sun in Figure 7(b), the detection of fluorescence signals is even more challenging, as shown in Figure 11(d). As discussed in Section 3.2, the fluorescence in mod-earth 0B is difficult to identify. Moreover, cloud coverage obscures the VRE features as well as the atmospheric features on exoplanets (Seager et al. 2005; Tinetti et al. 2006; Kaltenegger et al. 2007). The reflectance in Figure 12 indicates how clouds suppress the fluorescence signal. Even in the most optimistic model, the fluorescence in the reflectance is significantly reduced, and can hardly be observed. In the mod-earth model, it is impossible to identify the fluorescence signals. The only possible way to observe the surface vegetation, given significant cloud coverage, excluding atmospheric gases, would be via the VRE (∼0.1 in reflectance in the optimistic model). Thus, the existence of the water clouds that are expected for Earthlike planets with surface water seems to be critical for fluorescence detection. However, around TRAPPIST-1, as the relevant argument in Section 4.3.2 has shown, we found that the Chl fluorescence in the K I lines was insensitive to coverage by Earth clouds, which could be an advantage of Chl detection over BChl detection.

The fluorescence feature would be poorly determined with 900 hr of exposure time with 1σ errors, whereas the VRE feature could be identified. Even for a LUVOIR-A-like space telescope, an enormous amount of observational time would be needed to identify the fluorescence in addition to the VRE, with more confidence for detecting traces of photosynthesis. We

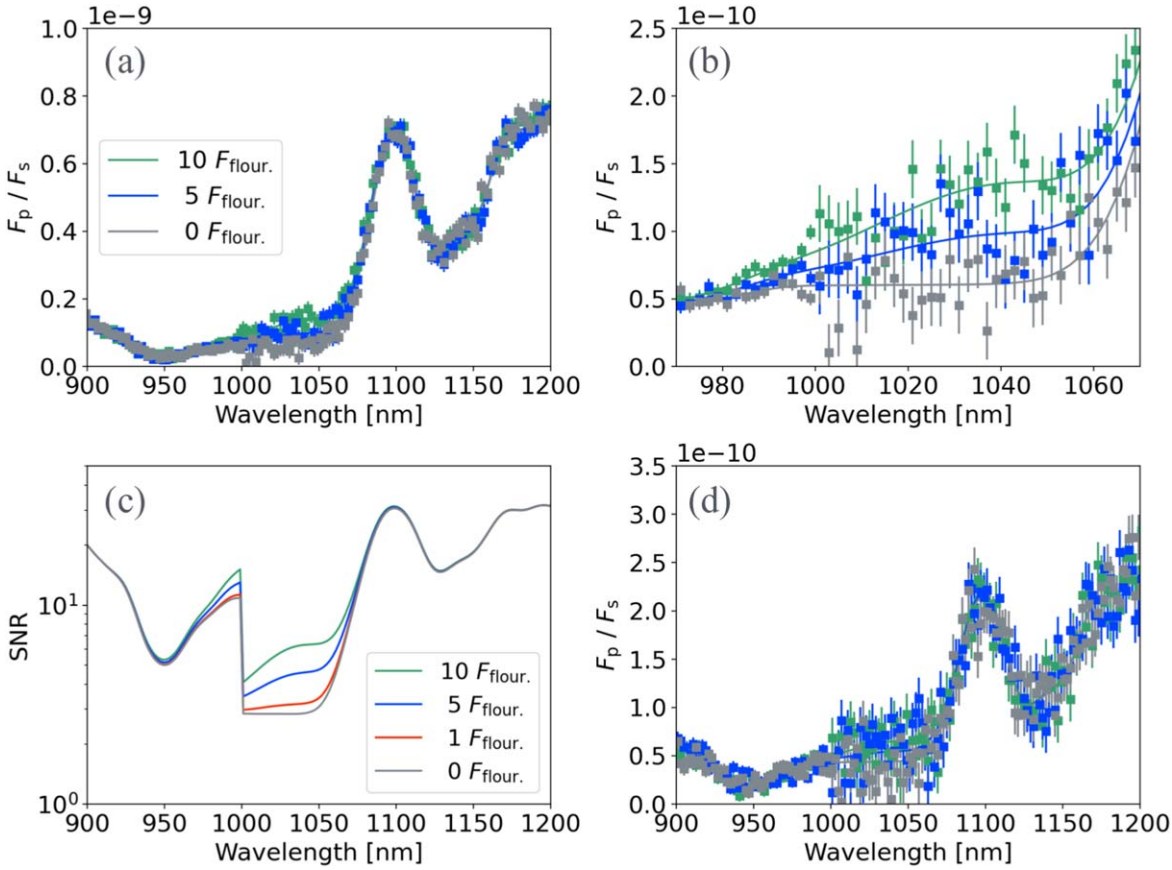

Figure 11. Simulated spectra with biological fluorescence on a second Earth around a Sunlike star at 10 pc from the Earth, assuming a LUVOIR-A-like space telescope. Panels (a)–(c) show the results from the veg-only 0B model, while panel (d) shows the results for F_p/F_s with the veg-land 0B model. (a) F_p/F_s with 9000 hr of observation time. The solid lines show the F_p/F_s and the error bars indicate the noise at each wavelength. (b) A magnification of the F_p/F_s in (a). (c) The S/N in (a).

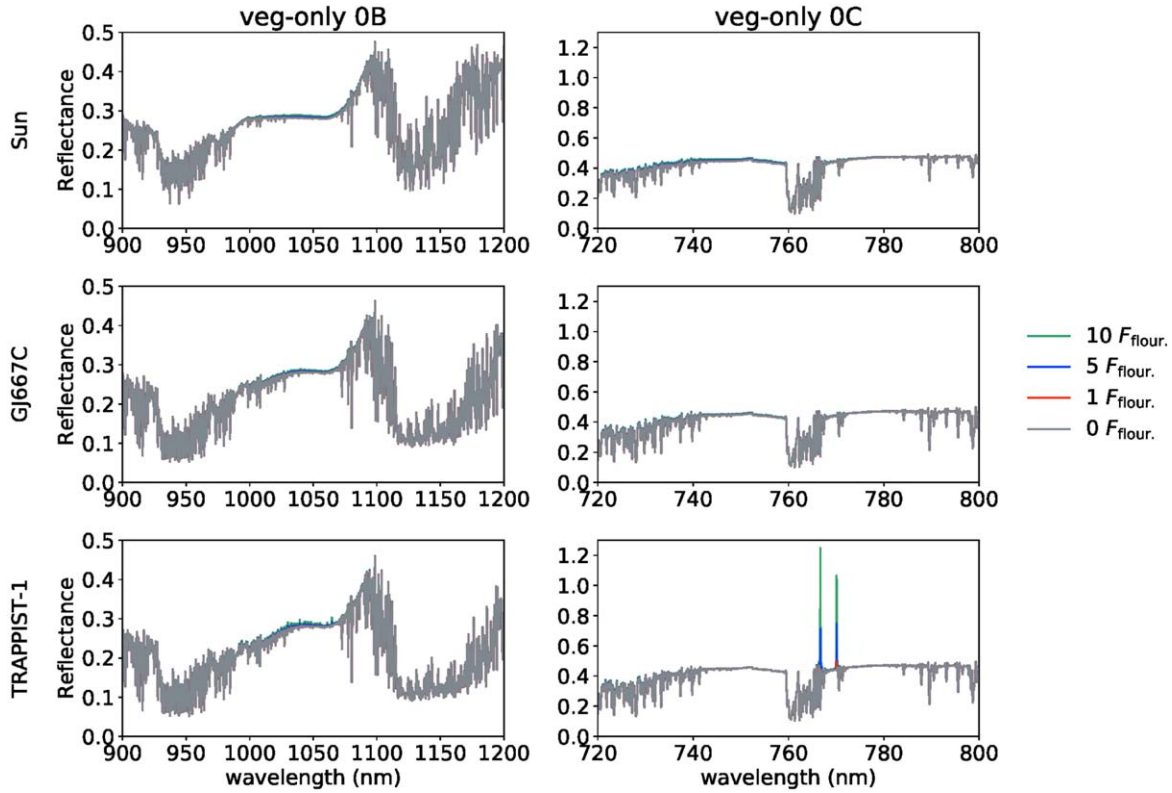

Figure 12. The effect of cloud coverage on the reflectance with the veg-only 0B and 0C models. The models are the same as the veg-only 0B model in Figure 7 and the veg-only 0C model in Figure 4, but with cloud coverage.

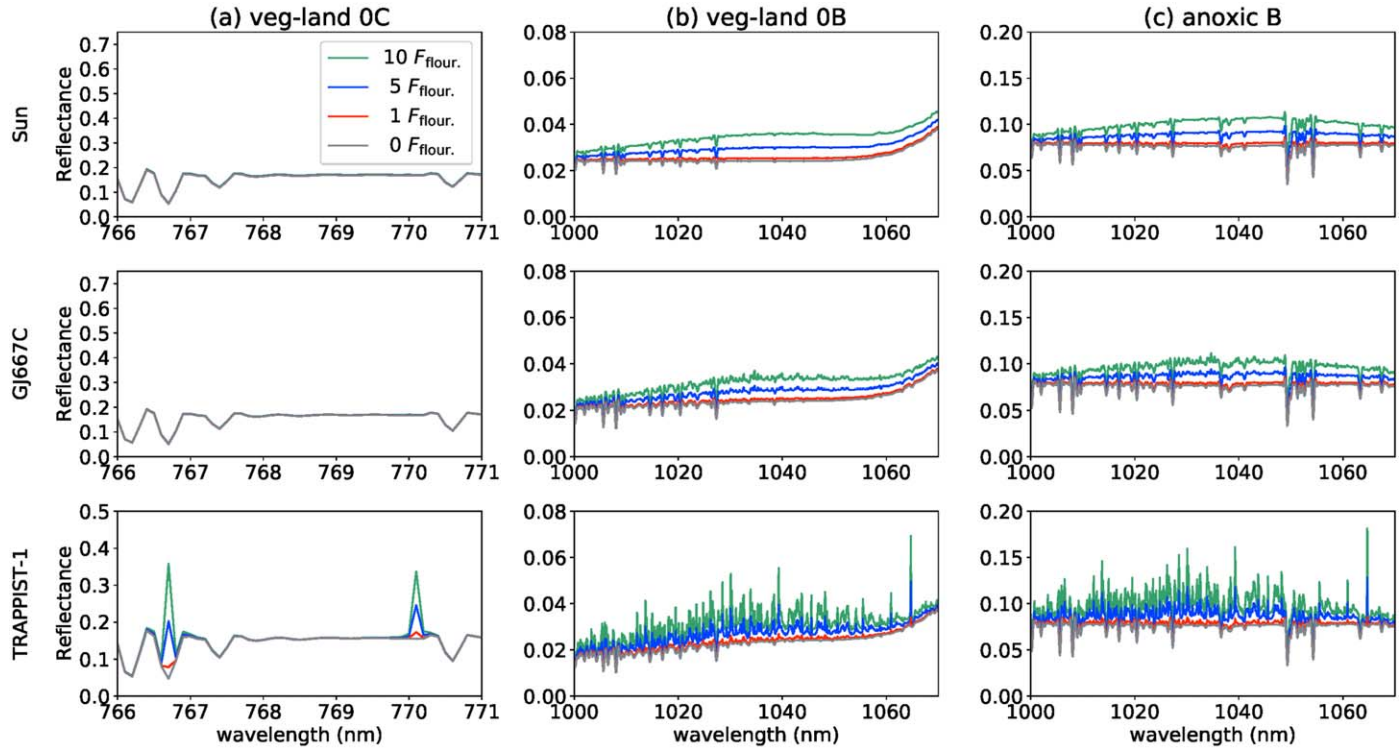

Figure 13. The apparent enhancement of fluorescence in the reflectance due to stellar absorption around three template stars: (a) the veg-only 0C model (Figure 4); (b) the veg-only 0B model (Figure 7); and (c) the anoxic B model (Figure 10).

also investigate the detectability of fluorescence using a space telescope with a different diameter. A 6 m space telescope is recommended for future space missions, according to the Astro2020 Decadal Survey. Using a 6 m diameter, ∼300,000 hr of observation time would be required to identify fluorescence. When we adopt a 30 m space telescope with 1σ errors, however, the required exposure time is reduced to ∼800 hr. Furthermore, one of the background noises—i.e., the readout noise—could be suppressed by data processing, due to the increasing readouts in exposure being implemented for H2RG IR detectors (e.g., Brandt et al. 2017; Kuzuhara et al. 2018). When the readout noise is assumed to be zero over all wavelengths, the required observation times are reduced to ∼250,000, ∼7000, and ∼500 hr with the 6, 15, and 30 m diameters, respectively.

4.3.2. Apparent Enhancement in Fluorescence around Ultracool Stars and Possible Detection with High-dispersion Spectroscopy

Figure 13 shows the contribution of the fluorescence around three host stars. Around TRAPPIST-1, the apparent enhancement in reflectance induced by fluorescence is significant compared to that around the other two stars, because TRAPPIST-1 has strong absorption features spanning the wavelengths of the fluorescence. Within the TRAPPIST-1 stellar absorption features, the reflected light from the planet is reduced, allowing the fluorescence emission to become a much larger fraction of the outgoing flux (reflected + fluorescence) at these wavelengths. This is analogous to the methodology of SIF detection with remote-sensing observations and retrieval processes that determine the extent to which the fluorescence influences the Fraunhofer lines (Maier et al. 2004). These spectroscopic features may be widely used for fluorescence detection around ultracool stars.

Figure 13(a) shows that the reflectance is highly enhanced by the absorption lines of K I in the stellar spectrum of TRAPPIST-1, which is not affected by water clouds (Figure 12). The degree of enhancement for each line depends on the atmospheric compositions of an Earthlike planet. Figures 13(b) and (c) present spiky features, due to the absorption of FeH and VO, as is commonly observed around ultracool stars. Therefore, observing the possible fluorescence signal at high spectral resolution, using extremely large ground telescopes, would be worthwhile.

5. Conclusions

In this paper, we have explored in great detail fluorescence from photosynthesis as a biosignature of exoplanets for future observations, and we have identified the situations in which this signal could be enhanced, as well as the regions of the spectrum where fluorescence from Chls and BChls could be most detectable for Earthlike planets around different stars. We have also described how we could enhance the possibility of detecting the action of photosynthesis more definitively. For direct imaging observations, however, we have found that the detection of fluorescence emissions would be extremely challenging to observe, and not feasible for the planned 6 m space telescope, in particular. More details are provided as follows.

We have considered fluorescence emissions from Chl- and BChl-based vegetation in clear sky conditions on an Earthlike planet around the Sun and two M dwarfs (GJ667 C and TRAPPIST-1). Chl- and BChl-based leaves show a VRE in wavelengths around 700–750 and 1000–1100 nm. The fluorescence emissions from Chls and BChls occur at wavelengths from 650 to 800 nm and 1000 to 1100 nm, corresponding to the longest Q absorption band of each

pigment. The two peaks of Chl fluorescence at 680 and 740 nm arise from the PSII and PSI, respectively. Thus, atmospheric absorption bands—such as H_2O, CH_4, O_2, and O_3—and the VRE could overlap the fluorescence emissions from Chls and BChls. The Chl fluorescence emission from PSI is blended with the steep VRE feature. The fluorescence emitted from PSII on an Earthlike planet is the most promising feature for observation, but it may also be reduced by nonphotochemical quenching processes and the reabsorption of photons by the surrounding Chls. Conversely, the fluorescence emitted from the BChls is not suppressed by the sharp increase in reflectance due to the VRE and atmospheric absorption by, for example, water vapor, except for the CH_4 absorption around 1000 nm. Therefore, the BChl fluorescence in the wavelength range of 1000–1100 nm, rather than the Chl fluorescence, may be a more promising biosignature from photosynthetic organisms on a planetary surface. In the cases of both Chl- and BChl-based vegetation, the simultaneous detection of the VRE and of fluorescence is significant for identifying photosynthetic activity on an exoplanet, because we do not know in principle exactly what kind of vegetation exists on the planet, and we need more information for further validation to identify the trace of photosynthesis. If BChl-bearing photosynthetic bacteria inhabit water without any leaf or tree structures, the fluorescence spectrum is the only surface reflectance feature that can be used to access such underwater photosynthetic organisms, although the fluorescence signal would be reduced, according to the opacity of the overlying liquid water.

Based on our understanding of photosynthesis, the intensity of the fluorescence is lower in photosynthetic bacteria compared to land plants. Here, we have presented four factors that enhance the fluorescence emission for the possible detection of biological fluorescence on an exoplanet: (1) increasing Chl/BChl concentration per the land area; (2) a small overlap of the absorption and fluorescence spectra; (3) low photosynthetic efficiency; and (4) the suppression of heat dissipation. This study has assumed a linear photoresponse of fluorescence to excitation light intensity. If a planet is on a large elliptical orbit, and the telescope has sufficient sensitivity to temporally resolve changes in fluorescence as a function of time, the nonlinear photoresponse from the biological fluorescence can be identified. Assuming a LUVOIR-A-like mission, an enormous period of time (around 9000 hr) would be required to detect BChl fluorescence emission, with the fluorescence yield being five to 10 times larger than that of the vegetation on Earth, in optimistic cases for an Earth–Sun twin at a distance of 10 pc from the Earth. In addition, cloud coverage significantly affects the detection of fluorescence, as well as other spectral features, because the cloud obscures fluorescence emissions more strongly than it does the VRE feature. Interestingly, the fluorescence in the reflectance was found to be remarkably enhanced in all three cases around TRAPPIST-1, because of its strong absorption in the stellar atmosphere, like SIF detection by remote sensing using Fraunhofer lines. The reflectance excess due to K I absorption and VO/FeH absorption could be a promising feature for characterizing the fluorescence around ultracool stars in the Chl and BChl cases. Note that Chl fluorescence in K I lines was still prominent with water clouds.

Thus, one of the most important future works would be a mock observation, assuming a 30 m class ground-based telescope, to investigate how the apparent enhancement in reflectance due to stellar absorption could help the detection of fluorescence around ultracool stars. In addition, to better support the future detection of fluorescence emissions on exoplanets, further studies are required from various perspectives. For example, planetary spectra for a wide range of atmospheric and surface conditions consistent with biological fluorescence emission should be estimated and tested using radiation transfer calculations, because our studies have considered conditions that remain limited. Moreover, we also need to conduct simulations of how the fluorescence is observed on an exoplanet when global SIF map data from the remote sensing of the Earth are applied. Further, experiments to validate prominent NIR fluorescence emissions are needed for some species of photosynthetic organisms and conditions.

We would like to thank the anonymous reviewer for the constructive comments for improving the paper. We also thank Tatsuya Miyauchi, Haruki Oshio, Yu Someya, Tomoki Kiyono, and Masanori Takeda for fruitful discussions at NIES on SIF detection by remote sensing, which led to the draft version of this study, and Kouki Hikosaka (Tohoku University) and Hibiki Noda (NIES) for further discussions and for introducing SIF identification by remote sensing. The data for the LUVOIR noise model were helpfully provided by Geronimo Villanueva and Ravi Kopparapu (NASA/Goddard). Y.H. and N.N. were supported by a Grant-in-Aid for Scientific Research on Innovative Areas (JSPS KAKENHI grant number 18H05439). PyAstronomy (https://github.com/sczesla/PyAstronomy) was used in mock observations assuming a space telescope. In several cases, numerical data were extracted from figures in published papers using WebPlotDigitizer (https://automeris.io/WebPlotDigitizer/).

Appendix A
Empirical Rayleigh Scattering

The effect of Rayleigh scattering is implemented empirically, as follows (Bucholtz 1995):

$$\tau_{\rm R}(\lambda) = \beta_{\rm s}(\lambda)\frac{T_{\rm s}}{P_{\rm s}}\int_0^{z'}\frac{P(z)}{T(z)}dz, \tag{A1}$$

where $\tau_{\rm R}$ is the Rayleigh optical depth at altitude z', and $T(z)$ and $P(z)$ are the temperature and pressure at z, respectively. We adopted the $T-P$ profile in the US standard atmosphere (1976), from 0 to 60 km, to compute the Rayleigh scattering cross section in the atmosphere of an Earthlike planet. The actual $T-P$ profile in the atmosphere of an Earthlike planet around a star other than the Sun is quite different from that in Earth's atmosphere. Rayleigh scattering, however, has a negligible effect on the transmittance at wavelengths from 600 to 1100 nm (≈6% in transmittance at 600 nm, reducing with increasing wavelength, then <1% at 1100 nm for an Earthlike planet around the Sun, for instance), which is closely related to the fluorescence from Chls and BChls. $T_{\rm s}$ and $P_{\rm s}$ are the temperature and pressure at standard conditions on Earth, respectively ($T_{\rm s} = 288.15$ K and $P_{\rm s} = 1013.25$ mbars). The total Rayleigh volume-scattering coefficient β_s is expressed as:

$$\beta_s(\lambda) = A\lambda^{-B-C\lambda-D/\lambda}, \tag{A2}$$

where the coefficients A, B, C, and D are empirically determined (see Table 3 in Bucholtz 1995).

Appendix B
LUVOIR Noise Model

We implemented a noise model assuming a LUVOIR-A-like mission. The formalism and the parameters are based on Robinson et al. (2016), but, as shown in Table 2, we have updated some parameters (with several treatments), following Kopparapu et al. (2021), for our simulations with the LUVOIR-A telescope.

The total noise in the observation $C_{\rm total}$ is calculated by:

$$C_{\rm total} = C_{\rm p} + C_{\rm s} + C_{\rm b}, \tag{B1}$$

where $C_{\rm p}$ is the number of planet photons, $C_{\rm s}$ is the stellar photon noise (the leakage through the coronagraph), and $C_{\rm b}$ is the background noise, which is the sum of the zodi $C_{\rm z}$, exozodi $C_{\rm ez}$, dark current $C_{\rm D}$, and readout noise $C_{\rm R}$. The internal thermal noise is ignored, because the thermal contribution is negligible in our wavelengths of interest. Note that the noise in Equation (B1) corresponds to the variance rather than the standard deviation. The noise count is expressed as:

$$C_{\rm noise} = \sqrt{C_{\rm p} + C_{\rm s} + 2C_{\rm b}}, \tag{B2}$$

where the double $C_{\rm b}$ accounts for the on–off observation with and without the planet. The on–off observation corresponds to the subtraction of the point-spread functions of a central star. The S/N for each wavelength λ is defined by:

$$\mathrm{S/N} = \frac{C_{\rm p}}{C_{\rm noise}}. \tag{B3}$$

The $F_{\rm p}$ and $F_{\rm s}$ are now defined as the reflected light from a planet and the stellar flux acquired by the telescope at a wavelength (bin) λ. When observing $F_{\rm p}/F_{\rm s}$, the 1σ error at λ is given as:

$$\sigma(\lambda) = \frac{F_{\rm p}}{F_{\rm s}}\frac{1}{\mathrm{S/N}}. \tag{B4}$$

The end-to-end throughput for planetary fluxes is calculated as:

$$T_{\rm total} = T_{\rm Tele}\,T_{\rm cor}\,T_{\rm opt}\,T_{\rm read}\,T_{\rm QE}, \tag{B5}$$

where $T_{\rm Tele}$ is accounts for the light lost due to contamination and inefficiencies in the main collecting area, $T_{\rm read}$ is the readout efficiency, and $T_{\rm QE}$ is the raw quantum efficiency for the detector. The coronagraphic $T_{\rm cor}$ and the optical $T_{\rm opt}$ throughputs are the same as those in Figure 9 in Kopparapu et al. (2021).

We have updated the formalism of the noise from zodis, exozodis, and readout as follows. In Robinson et al. (2016), the spectral shape of the zodis (exozodis) was assumed to be equal to that of the Sun (the host star). Instead, we explicitly adopt the normalized reflectance on solar zodis, $\tilde{R}_{\odot,\lambda}$, in the model, to better account for the zodiacal light in a exoplanetary system. We calculate $\tilde{R}_{\odot,\lambda}$ by tracing the spectral data from observations of the zodiacal light (see Figure 8 in Kawara et al. 2017 and Figure 10 in Tsumura et al. 2010), with the normalization in the V band. Using $\tilde{R}_{\odot,\lambda}$, the noise from the zodis is expressed as:

$$C_{\rm z} = \frac{\pi\lambda^2 D^2}{4hcR}\frac{F_{\odot,\lambda}\,(1\ \mathrm{au})}{F_{\odot,V}\,(1\ \mathrm{au})} \times \tilde{R}_{\odot,\lambda}F_{0,V}10^{-M_{\mathrm{z},V}/2.5}T_{\rm total}\,\Omega\Delta t_{\rm exp}, \tag{B6}$$

where $F_{\odot,\lambda}$ is the solar flux density at λ, $F_{\odot,V}$ is the solar flux density in the V band, h is the Planck constant, c is the speed of light, $M_{\mathrm{z},V} = 23$ mag arcsec^{-2} is the V-band zodiacal light surface brightness, and $\Delta t_{\rm exp}$ is the exposure time. The circular photometry aperture size is expressed as $\Omega = \pi(X\lambda/D)^2$. Assuming the reflectance of the exozodis to be the same as $\tilde{R}_{\odot,\lambda}$, the noise from the exozodis is written as:

$$C_{\rm ez} = \frac{\pi\lambda^2 D^2}{4hcR}\left(\frac{1\ \mathrm{au}}{r}\right)^2\frac{F_{\mathrm{s},\lambda}\,(1\ \mathrm{au})}{F_{\mathrm{s},V}\,(1\ \mathrm{au})} \times \frac{F_{\mathrm{s},V}\,(1\ \mathrm{au})}{F_{\odot,V}\,(1\ \mathrm{au})}\tilde{R}_{\odot,\lambda}F_{0,V}N_{\rm ez}10^{-M_{\mathrm{ez},V}/2.5}T_{\rm total}\,\Omega\Delta t_{\rm exp}, \tag{B7}$$

where $F_{\mathrm{s},\lambda}$ is the stellar flux density at λ, $F_{\mathrm{s},V}$ is the stellar flux density in the V band, and r is the distance between the planet and the parent star. $M_{\mathrm{ez},V} = 22$ mag arcsec^{-2} is the V-band exozodiacal light surface brightness. Even if the original treatment of exozodiacal light is adopted, our results do not significantly vary. We calculate the readout noise ($C_{\rm R}$) to be $C_{\rm R} = N_{\rm pix}N_{\rm read}R_{\rm e^-}^2$, instead of $C_{\rm R} = N_{\rm pix}N_{\rm read}R_{\rm e^-}$ as in Robinson et al. (2016), to more realistically incorporate the noise propagation, where $N_{\rm pix}$ is the number of contribution pixels, $N_{\rm read}$ is the number of reads at each observation, and $R_{\rm e^-}$ is the read noise count.

Table 2
Parameters for Simulations Based on a LUVOIR-A-like Mission

Parameter	Description	Adopted Value
D	Mirror diameter	6, 15, 30 m
C	Raw contrast	10^{-10}
R	Instrumental spectral resolution	70
$T_{\rm Tele}$	To account for light lost due to contamination and inefficiencies in the main collecting area	0.95
$T_{\rm read}$	Readout efficiency	0.75
$T_{\rm QE}$	Raw quantum efficiency	0.9
$f_{\rm pa}$	Fraction of planetary light that falls within the photometric aperture	1
X	Width of the photometric aperture as multiple of λ/D	0.″61
$N_{\rm ez}$	Number of exozodis	4.5
D_{e-}	Dark current (UVIS/NIR)	3E-5/2E-3 $\mathrm{e^-\ s^{-1}}$
R_{e-}	Read noise per pixel (UVIS/NIR)[a]	0/2.5 $\mathrm{e^-}$
$\theta_{\rm IWA}$	Inner working angle of the coronagraph as a multiple of λ/D	3
λ_0	Diffraction limit at the wavelength	500 nm

Note.
[a] Taken from the Planetary Spectrum Generator for LUVOIR/A-VIS and A-NIR, which is maintained by NASA (https://psg.gsfc.nasa.gov/instrument.php).

ORCID iDs

Yu Komatsu https://orcid.org/0000-0002-0371-2885
Yasunori Hori https://orcid.org/0000-0003-4676-0251
Masayuki Kuzuhara https://orcid.org/0000-0002-4677-9182
Makiko Kosugi https://orcid.org/0000-0002-7415-1536

Kenji Takizawa https://orcid.org/0000-0002-1060-5738
Norio Narita https://orcid.org/0000-0001-8511-2981
Masashi Omiya https://orcid.org/0000-0002-5051-6027
Eunchul Kim https://orcid.org/0000-0003-3380-3953
Nobuhiko Kusakabe https://orcid.org/0000-0001-9194-1268
Victoria Meadows https://orcid.org/0000-0002-1386-1710
Motohide Tamura https://orcid.org/0000-0002-6510-0681

References

Allen-Sutter, H., Garhart, E., Leinenweber, K., et al. 2020, PSJ, 1, 39
Baker, N. R. 2008, Annu. Rev. Plant Biol., 59, 89
Baldridge, A., Hook, S., Grove, C., & Rivera, G. 2009, RSEnv, 113, 711
Bishop, J. L., Bell, J. F., III, Bell, J., & Moersch, J. E. 2019, Remote Compositional Analysis: Techniques for Understanding Spectroscopy, Mineralogy, and Geochemistry of Planetary Surfaces (Cambridge: Cambridge Univ. Press)
Brandt, T. D., Rizzo, M., Groff, T., et al. 2017, JATIS, 3, 048002
Bucholtz, A. 1995, ApOpt, 34, 2765
Callies, J., Corpaccioli, E., Eisinger, M., Hahne, A., & Lefebvre, A. 2000, ESABu, 102, 28
Cogdell, R. J. 1978, RSPTA, 284, 569
Des Marais, D. J., Harwit, M. O., Jucks, K. W., et al. 2002, AsBio, 2, 153
Du, S., Liu, L., Liu, X., et al. 2019, Sensors, 19, 3009
Du, S., Liu, L., Liu, X., & Hu, J. 2017, RemS, 9, 911
Feret, J.-B., François, C., Asner, G. P., et al. 2008, RSEnv, 112, 3030
France, K., Loyd, R. P., Youngblood, A., et al. 2016, ApJ, 820, 89
Frankenberg, C., O'Dell, C., Berry, J., et al. 2014, RSEnv, 147, 1
Frankenberg, C., O'Dell, C., Guanter, L., & McDuffie, J. 2012, AMT, 5, 2081
Fujita, Y., & Ohki, K. 2004, Plant Cell Physiol., 45, 392
Gao, B.-C., & Kaufman, Y. J. 2003, JGRD, 108, 4389
Gates, K., & Schleter, W. 1965, ApOpt, 4, 11
Genty, B., Briantais, J.-M., & Baker, N. R. 1989, Biochim. Biophys. Acta General Subjects, 990, 87
Grimm, B., Porra, R. J., Rüdiger, W., et al. 2006, Chlorophylls and Bacteriochlorophylls: Biochemistry, Biophysics, Functions and Applications (Dordrecht: Springer)
Guanter, L., Alonso, L., Gómez-Chova, L., et al. 2010, JGRD, 115, D19303
Hamazaki, T., Kaneko, Y., Kuze, A., & Kondo, K. 2005, Proc. SPIE, 5659, 73
Huete, A., Didan, K., Miura, T., et al. 2002, RSEnv, 83, 195
Jackson, C. T., Jeong, S., Dorlhiac, G. F., & Landry, M. P. 2021, iSci, 24, 102156
Jacquemoud, S., & Baret, F. 1990, RSEnv, 34, 75
Kaltenegger, L., Traub, W. A., & Jucks, K. W. 2007, ApJ, 658, 598
Kasting, J. F., & Ackerman, T. P. 1986, Sci, 234, 1383
Kawara, K., Matsuoka, Y., Sano, K., et al. 2017, PASJ, 69, 31
Kiang, N. Y., Segura, A., Tinetti, G., et al. 2007a, AsBio, 7, 252
Kiang, N. Y., Siefert, J., & Blankenship, R. E. 2007b, AsBio, 7, 222
Klima, R. L., Dyar, M. D., & Pieters, C. M. 2011, M&PS, 46, 379
Köhler, P., Fischer, W. W., Rossman, G. R., et al. 2021, GeoRL, 48, e2021GL095227
Kopparapu, R., Arney, G., Haqq-Misra, J., Lustig-Yaeger, H., & Villanueva, G. 2021, ApJ, 908, 164
Kosugi, M., Ozawa, S.-I., Takahashi, Y., et al. 2020, Biochim. Biophys. Acta Bioenergetics, 1861, 148139
Kotabová, E., Jarešová, J., Kaňa, R., et al. 2014, Biochim. Biophys. Acta Bioenergetics, 1837, 734
Krause, G., & Weis, E. 1991, Annu. Rev. Plant Biol., 42, 313
Kuzuhara, M., Hirano, T., Kotani, T., et al. 2018, Proc. SPIE, 10702, 1070260
Lakowicz, J. R. 2006, Principles of Fluorescence Spectroscopy (Berlin: Springer)
Lee, J.-E., Frankenberg, C., van der Tol, C., et al. 2013, RSPSB, 280, 20130171
Lehmer, O. R., Catling, D. C., Parenteau, M. N., Kiang, N. Y., & Hoehler, T. M. 2021, FrASS, 8, 111
Lincowski, A. P., Meadows, V. S., Crisp, D., et al. 2018, ApJ, 867, 76
Livengood, T. A., Deming, L. D., A'hearn, M. F., et al. 2011, AsBio, 11, 907
Magdaong, N. C. M., Niedzwiedzki, D. M., Goodson, C., & Blankenship, R. E. 2016, JPCB, 120, 5159
Maier, S. W., Günther, K. P., & Stellmes, M. 2004, Digital Imaging and Spectral Techniques: Applications to Precision Agriculture and Crop Physiology (New York: Wiley), 209
Meadows, V. S., Reinhard, C. T., Arney, G. N., et al. 2018, AsBio, 18, 630
Meftah, M., Damé, L., Bolsée, D., et al. 2018, A&A, 611, A1
Montañés-Rodríguez, P., Pallé, E., Goode, P., & Martín-Torres, F. 2006, ApJ, 651, 544
Nakajima, M., Kuze, A., & Suto, H. 2012, Proc. SPIE, 8533, 853306
O'Malley-James, J. T., & Kaltenegger, L. 2018, MNRAS, 481, 2487
O'Malley-James, J. T., & Kaltenegger, L. 2019, MNRAS, 488, 4530
Pavlov, A., & Kasting, J. 2002, AsBio, 2, 27
Porcar-Castell, A., Aalenovský, Z., Magney, T., et al. 2021, Nat. Plants, 7, 998
Robinson, T. D., Stapelfeldt, K. R., & Marley, M. S. 2016, PASP, 128, 025003
Rugheimer, S., & Kaltenegger, L. 2018, ApJ, 854, 19
Sanromá, E., Pallé, E., Parenteau, M., et al. 2013, ApJ, 780, 52
Schirhagl, R., Chang, K., Loretz, M., & Degen, C. L. 2014, ARPC, 65, 83
Schuurmans, R. M., van Alphen, P., Schuurmans, J. M., Matthijs, H. C., & Hellingwerf, K. J. 2015, PLoSO, 10, e0139061
Schwieterman, E. 2018, Handbook of Exoplanets (Cham: Springer), 69
Schwieterman, E. W., Cockell, C. S., & Meadows, V. S. 2015, AsBio, 15, 341
Schwieterman, E. W., Kiang, N. Y., Parenteau, M. N., et al. 2018, AsBio, 18, 663
Seager, S., Turner, E. L., Schafer, J., & Ford, E. B. 2005, AsBio, 5, 372
Segura, A., Kasting, J. F., Meadows, V., et al. 2005, AsBio, 5, 706
Selvaggio, G., Chizhik, A., Nißler, R., et al. 2020, NatCo, 11, 1495
Sun, Y., Frankenberg, C., Jung, M., et al. 2018, RSEnv, 209, 808
Sunshine, J. M., & Pieters, C. M. 1998, JGR, 103, 13675
Takizawa, K., Minagawa, J., Tamura, M., Kusakabe, N., & Narita, N. 2017, NatSR, 7, 7561
Tinetti, G., Meadows, V. S., Crisp, D., et al. 2006, AsBio, 6, 881
Tsumura, K., Battle, J., Bock, J., et al. 2010, ApJ, 719, 394
Wilhelm, C., & Jakob, T. 2006, Photosynth. Res., 87, 323
Wolf, B. M., Niedzwiedzki, D. M., Magdaong, N. C. M., et al. 2018, Photosynth. Res., 135, 177
Yao, L., Yang, D., Liu, Y., et al. 2021, AdAtS, 38, 341